

ISOPARAMETRIC UNFITTED BDF – FINITE ELEMENT METHOD FOR PDES ON EVOLVING DOMAINS *

YIMIN LOU[†] AND CHRISTOPH LEHRENFELD[‡]

Abstract. We propose a new discretization method for PDEs on moving domains in the setting of unfitted finite element methods, which is provably higher-order accurate in space and time. In the considered setting, the physical domain that evolves essentially arbitrarily through a time-independent computational background domain, is represented by a level set function. For the time discretization, the application of standard time stepping schemes that are based on finite difference approximations of the time derivative is not directly possible, as the degrees of freedom may get active or inactive across such a finite difference stencil in time. In [Lehrenfeld, Olshanskii. An Eulerian finite element method for PDEs in time-dependent domains. ESAIM: M2AN, 53:585–614, 2019] this problem is overcome by extending the discrete solution at every timestep to a sufficiently large neighborhood so that all the degrees of freedom that are relevant at the next time step stay active. But that paper focuses on low-order methods. We advance these results with introducing and analyzing realizable techniques for the extension to higher order. To obtain higher-order convergence in space and time, we combine the BDF time stepping with the isoparametric unfitted FEM. The latter has been used and analyzed for several stationary problems before. However, for moving domains the key ingredient in the method, the transformation of the underlying mesh, becomes time-dependent which gives rise to some technical issues. We treat these with special care, carry out an a priori error analysis and two numerical experiments.

Key words. Eulerian time stepping, isoparametric FEM, unfitted FEM, evolving domains, ghost penalty, stabilization, higher order FEM, BDF, projection errors

AMS subject classifications. 65M12, 65M60, 65M85

1. Introduction. Partial differential equations (PDEs) posed on time-dependent domains appear in many problems in physics, chemistry, biology and engineering. Famous problem classes of that sort are two-phase flow and free surface problems. In recent years, geometrically unfitted finite element methods (FEM) such as CutFEM [2] have become very popular. In these methods, the geometry is described separately from the computational background mesh, which allow us to handle domains that may exhibit strong deformations or even topology changes. In the following we represent the physical domains, embedded and evolving smoothly in a time-independent background domain, implicitly by a level set function. While for PDEs on stationary domains, suitable unfitted finite element methods have been designed, analyzed, implemented and validated for a broad range of problems, the treatment of unfitted moving domains is less well-explored. A method-of-lines approach is not directly applicable as the domain of definition of the discrete solution and hence the corresponding unfitted finite element space changes between time instances. There are (at least) three approaches to solving this problem:

1. In [8] and very recently in [4] a *characteristic Galerkin* or *semi-Lagrangian* formulation for a convection-diffusion problem on an evolving surface and an evolving bulk domain have been considered, respectively. Here, instead of discretizing the partial time derivative ∂_t , the material derivative is used and approximated by

*Submitted to the editors DATE.

Funding: This work was funded by the German Science Foundation (DFG) within the project "LE 3726/1-1".

[†]Institute for Numerical and Applied Mathematics, University of Göttingen, Germany (lou@math.uni-goettingen.de).

[‡]Institute for Numerical and Applied Mathematics, University of Göttingen, Germany (lehrenfeld@math.uni-goettingen.de).

backtracking trajectories at required integration points.

2. A space-time reformulation of the problem with a moving domain allows to transfer the main concepts of unfitted FEM from the case of stationary to that of time-dependent domains. Such an approach has been considered, e.g., in [18, 13] for scalar interface problems and recently extended to higher order in space and time in [23, 10]. A variant that reduces the complexity that comes with a space-time formulation is the quadrature-in-time approach introduced in [27] and applied in [9, 6].

3. An alternative strategy stays in the framework of the usual method of lines. To this end, an extension is applied at every time step to make previous solutions well-defined in subsequent time steps. Without analysis and with the restriction of applying the extension to direct neighbors only, such a strategy has been considered in [25]. And in [17], for scalar problems, this approach has been generalized, studied more systematically and put on a mathematically rigorous foundation. Developments to unsteady Stokes problems on moving domains have been considered in [3, 26].

In this paper, we restrict ourselves to the third class of methods and extend [17] with respect to two major limitations. First of all, in [17] only an implicit Euler time discretization has been analyzed, while we upgrade this to the Backward Differentiation Formulas (BDF) for higher order of accuracy (with focus on BDF2 in the analysis). The second limitation of [17] that we remove, is the abstract assumption of an arbitrarily accurate geometry handling. In [17] it is assumed that the domain integrals on the implicitly – through level set functions – described geometries can be carried out robustly and arbitrarily accurate. In practice, however, this is hard to achieve. Existing strategies for numerical integration on the cut geometries are typically either low-order accurate or fail to guarantee positive quadrature weights and hence stable quadrature. In [15] the concept of geometrically unfitted *isoparametric* finite elements has been introduced as a remedy to combine guaranteed positive quadrature weights with arbitrarily accurate numerical integration on smooth domains. Afterwards, this approach has been successfully applied and analyzed to several *stationary* problems in a.o. [20, 19, 12, 16, 7]. To obtain a computationally feasible but still higher-order accurate approach for the handling of the implicit geometry, we also consider the use of the isoparametric unfitted FEM in this work, but in the context of moving domain.

Content and structure of the paper. The major contribution in this work is the development of the method in [17] to higher order of accuracy. This includes:

- Introduction of an arbitrarily high order in space and first to third order in time method for a scalar convection-diffusion equation on an evolving domain.
- Handling and estimates for mesh deformations changing in time in the isoparametric unfitted FEM. These results are valuable not only for the considered BDF-based time stepping schemes, and play a major part of this work.
- A priori error analysis of the BDF2-based method that yields arbitrarily high order of accuracy in space and up to second-order convergence in time.
- Numerical examples that confirms the predicted convergence rates and applications beyond the scope of the considered numerical analysis.

This paper is organized as follows. In [Section 2](#) we introduce the PDE problem. In preparation of the definition of the method, in [Section 3](#) we gather notation and properties of the computational mesh, its time-dependent active parts, the isoparametric mesh transformation and a preliminary description of a transfer operator between different meshes. In [Section 4](#) the discretizations in space and time are given. The transfer operator is discussed in more detail in [Section 5](#) and several important results on the transfer operator are stated. Together with [Section 6](#) where the a priori error

analysis for the scheme is carried out, these two sections represent the most important pieces of this study. The main part of the paper concludes with [Section 7](#) that validates the theoretical findings and extends beyond them. This manuscript requires a significant amount of notation. To facilitate working with the many different symbols we make heavy use of the hyperlink capabilities of pdf documents.

2. Mathematical model. For ease of presentation we mainly consider the convection-diffusion equation posed on an evolving domain. The method, however, has been verified feasible for some more complicated models, such as two-phase interface problem tested in [Section 7](#) or unsteady incompressible flows in [[3](#), [26](#)], and with some restriction on the time step size also in [[25](#)].

Let $\Omega(t) \subset \mathbb{R}^d$, $d = 2, 3$, be a time-dependent domain with Lipschitz boundary $\Gamma := \partial\Omega$ evolving in a time interval $t \in [0, \mathbf{T}]$, $\mathbf{T} \in \mathbb{R}_+$, which is embedded in a polygonal, time-independent background domain $\tilde{\Omega}$. For instance, $\Omega(t)$ may be regarded as a volume of fluid under motion and deformation, with a material velocity field of particles $\mathbf{w} : \tilde{\Omega} \rightarrow \mathbb{R}^d$ that has a proper meaning on the whole background domain $\tilde{\Omega}$. The conservation of a scalar quantity $u(\mathbf{x}, t)$ of the fluid with a diffusive flux is governed by

$$(2.1) \quad \partial_t u + \nabla \cdot (u\mathbf{w} - \nu\nabla u) = g \quad \text{in } \Omega(t), \quad \nabla u \cdot \mathbf{n} = 0 \quad \text{on } \Gamma(t), \quad t \in (0, \mathbf{T}),$$

where $\nu > 0$ denotes the diffusion coefficient, g is a source term and $\mathbf{n}(\mathbf{x}, t)$ is the unit normal on $\Gamma(t) = \partial\Omega(t)$. Here, for the sake of simplicity we apply boundary conditions that ensure the global conservation of u in $\Omega(t)$. For the treatment of Dirichlet-type boundary conditions or interface conditions using Nitsche's method we refer to [[26](#)] and the numerical examples. Further, we assume proper given initial conditions $u(\mathbf{x}, 0) = u_0(\mathbf{x})$ in $\Omega(0)$.

In order to describe the time-dependent domain $\Omega(t)$, a level set function $\phi(\mathbf{x}, t) : \tilde{\Omega} \times [0, \mathbf{T}] \rightarrow \mathbb{R}$ is utilized such that the boundary of the domain is represented by the zero level and the domain is described by the negative levels, i.e.

$$(2.2) \quad \Omega(t) = \{\mathbf{x} \in \tilde{\Omega} : \phi(\mathbf{x}, t) < 0\}, \quad \text{s.t. } \Gamma(t) = \{\mathbf{x} \in \tilde{\Omega} : \phi(\mathbf{x}, t) = 0\}.$$

In addition, we define an ϵ -neighborhood of the domain $\Omega_\epsilon(t) := \{\mathbf{x} \in \tilde{\Omega} : \phi(\mathbf{x}, t) < \epsilon\}$ for some $\epsilon > 0$ corresponding space-time domains

$$(2.3) \quad Q := \bigcup_{t \in (0, \mathbf{T})} \Omega(t) \times \{t\}, \quad Q_\epsilon := \bigcup_{t \in (0, \mathbf{T})} \Omega_\epsilon(t) \times \{t\}, \quad Q \subset Q_\epsilon \subset \mathbb{R}^{d+1}.$$

3. Preliminaries for the discretization. For the problem discussed in [Section 2](#) we seek a proper discretization using an *isoparametric unfitted finite element method* based on *volumetric discrete extensions* as in [[17](#)]. Here, a backward differentiation formula (BDF) for time stepping is coupled with a ghost penalty extension on top of an unfitted finite element discretization in space.

In this section we prepare notation, concepts, and assumptions for the definition of the method given in [Section 4](#), especially w.r.t. the geometrical approximation, finite element spaces and active meshes. In [Subsection 3.1](#) we define notation w.r.t. time discretization and the geometrical approximation with using a parametric mesh transformation. The properties of the isoparametric mapping are then summarized in [Subsection 3.3](#) and [Subsection 3.4](#). Further notation for active meshes and discrete neighborhoods is introduced in [Subsection 3.2](#).

3.1. Finite element spaces and geometrical approximation. First of all, we introduce notation for the discrete time levels of the time stepping procedure. Let $\Delta t := \mathbf{T}/N$, $N \in \mathbb{N}$ be the uniform time step of an equally-spaced subdivision of the time interval $(0, \mathbf{T}]$ under investigation. Let $t_n := n\Delta t$ be a time instance, then we denote by quantities with upper index n the corresponding quantity with restriction $t = t_n$, e.g. $\Omega^n := \Omega(t_n)$, $\Gamma^n := \Gamma(t_n)$, $\phi^n := \phi(\cdot, t_n)$, or $\Omega_\epsilon^n := \Omega_\epsilon(t_n)$, $n = 0, \dots, N$.

Let $\{\mathcal{T}_h\}$ be an admissible quasi-uniform family of simplicial triangulations with a diameter $h > 0$ on the background domain $\tilde{\Omega}$. On each of these triangulations \mathcal{T}_h we define the time-independent, standard finite element space with polynomials of order k as

$$(3.1) \quad \mathcal{V}_h = \mathcal{V}_h^{(k)} := \{v_h \in C(\tilde{\Omega}) : v_h|_T \in \mathcal{P}_k(T), \forall T \in \mathcal{T}_h\}.$$

Remark 3.1 (Inequalities up to constants). In order to simplify the inequalities with generic constants c that are independent of the mesh size h , time step Δt and time t_n , in the following $x \lesssim y$ ($x \gtrsim y$) denotes $x \leq cy$ ($x \geq cy$), and $x \simeq y$ indicates $x \lesssim y$ and $x \gtrsim y$. The hidden constant c may be referred to by $c_{(\mathbf{x}, \mathbf{y})}$ where (\mathbf{x}, \mathbf{y}) is the label of the corresponding inequality using the \lesssim or \gtrsim notation.

In general, for $n = 0, \dots, N$, only a good approximation $\phi_h^n \in \mathcal{V}_h^{(q)}$, $q \geq 1$, e.g., a higher-order piecewise polynomial approximation to ϕ^n , is given. We assume that $\partial\Omega^n$ is sufficiently smooth and

$$(3.2) \quad \text{dist}(\partial\Omega^n, \partial\Omega_{\phi_h^n}^n) \lesssim h^{q+1}, \quad \forall t \in [0, \mathbf{T}]$$

holds for $\Omega_{\phi_h^n}^n := \{\mathbf{x} \in \tilde{\Omega} \mid \phi_h^n(\mathbf{x}) < 0\}$. A well-known issue with the implicit description of the level set functions is that realizations of quadrature rules that preserve the geometrical order of accuracy are difficult to achieve, cf. the discussion in [15]. In the remainder of this work we consider the *isoparametric* approach introduced in [15] to tackle this problem. The underlying idea is that an only second-order approximation of $\Omega_{\phi_h^n}^n$ based on the piecewise linear interpolation $\hat{\phi}_h^n$ of ϕ_h^n simplifies the realization of quadrature rules dramatically. This configuration then serves as a reference configuration on which quadrature rules can easily be constructed (e.g., by simple geometrical decomposition rules). To improve the accuracy of this low-order approximation $\Omega_{\hat{\phi}_h^n}^n$ an additional transformation $\Theta_n \in [\mathcal{V}_h^{(q)}]^d$ is constructed at each time step n such that

$$(3.3) \quad \text{dist}(\partial\Omega^n, \Theta^n(\partial\Omega_{\hat{\phi}_h^n}^n)) \lesssim \text{dist}(\partial\Omega^n, \partial\Omega_{\phi_h^n}^n) + \text{dist}(\partial\Omega_{\phi_h^n}^n, \Theta^n(\partial\Omega_{\hat{\phi}_h^n}^n)) \lesssim h^{q+1}.$$

This transformation is itself a finite element function w.r.t. the (undeformed) background mesh which renders the task of accurate numerical integration feasible. The deformation is *local*, i.e., only in the vicinity of cut elements it deviates from the identity, and *small* everywhere in the sense that $\|\Theta^n\|_\infty \lesssim h^2$ (in detail [Subsection 3.3](#)). However, the fact that the deformed meshes and the properly adapted finite element spaces are in general time-dependent, results in several technicalities as we will see. Based on this configuration we define the high-order approximations of geometry, the deformed meshes and the time-dependent finite element spaces as (with $\Theta^{-n} := (\Theta^n)^{-1}$)

$$(3.4) \quad \Omega_h^n := \Theta^n(\Omega_{\hat{\phi}_h^n}^n), \quad \Gamma_h^n := \partial\Omega_h^n, \quad \mathcal{T}_h^n := \Theta^n(\mathcal{T}_h), \quad \mathcal{V}_h^n := \mathcal{V}_h \circ \Theta^{-n}.$$

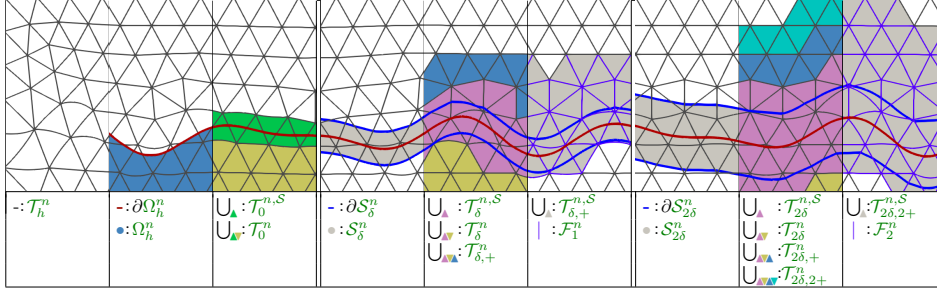


FIG. 3.1. Sketch of discrete domains and different selections of elements and facets. The first three columns display the mesh, the discrete domain Ω_h^n and the set of interior and cut elements. The three columns in the center display a strip domain related to an extension by δ and a corresponding element and facet selection while in the last three columns an extension by 2δ is considered.

3.2. Discrete neighborhoods and active meshes. As usual in unfitted finite element methods, only a part of the background mesh is involved in the computation at each time step. We therefore define *active* parts of meshes and finite element spaces as those parts corresponding to the elements that overlap the physical domain $\Omega(t)$ or its *discrete* δ -neighborhood. We refer to Figure 3.1 for a sketch of the different domains and meshes introduced next. First, let us define a *discrete* δ -strip for some $\delta \in \mathbb{R}_+$,

$$(3.5) \quad \mathcal{S}_\delta^n := \Theta^n \left(\Omega_{\phi_h - \delta}^n \setminus \Omega_{\phi_h + \delta}^n \right)$$

and the corresponding part of the set of elements and the corresponding domain

$$(3.6) \quad \mathcal{T}_\delta^{n,S} := \{T \in \mathcal{T}_h^n \mid \text{meas}_d(T \cap \mathcal{S}_\delta^n) > 0\}, \quad \mathcal{O}_\delta^{n,S} := \{\mathbf{x} \in \bar{T}, T \in \mathcal{T}_\delta^{n,S}\}.$$

Note that $\mathcal{T}_0^{n,S}$ and $\mathcal{O}_0^{n,S}$ denote the set of all *cut elements* and the corresponding domain, respectively, i.e., the elements that are cut by the discrete boundary $\partial\Omega_h$. For the discrete extension of the domain that includes the domain interior, the *active* part of the mesh and its domain we have

$$(3.7) \quad \Omega_\delta^n := \Theta^n(\Omega_{\phi_h - \delta}^n), \mathcal{T}_\delta^n := \{T \in \mathcal{T}_h^n \mid \text{meas}_d(T \cap \Omega_\delta^n) > 0\}, \mathcal{O}_\delta^n := \{\mathbf{x} \in \bar{T}, T \in \mathcal{T}_\delta^n\}.$$

Corresponding to \mathcal{T}_δ^n we define the time-dependent finite element spaces on the *active meshes* as continuous, piecewise mapped polynomials of degree k :

$$(3.8) \quad \mathcal{V}_\delta^n := \mathcal{V}_h^n|_{\mathcal{O}_\delta^n} = \{v_h \in C(\mathcal{O}_\delta^n) : v_h|_T \in \mathcal{P}_k(T) \circ \Theta^{-n}, \forall T \in \mathcal{T}_\delta^n\}.$$

We furthermore add a subscript “+” to expand a set of elements or domain by all neighboring elements¹, e.g., the neighboring elements in addition to the cut elements are denoted by $\mathcal{T}_{0,+}^n$. This extension can also be stacked r times², e.g., $\mathcal{T}_{\delta,2+}^n := \mathcal{T}_{\delta,+}^n$ and $\mathcal{O}_{\delta,3+}^n := \mathcal{O}_{\delta,+++}^n$. Obviously, there holds

$$(3.9) \quad \text{dist} \left(\mathcal{O}_{r\delta,r+}^n, \mathcal{O}_0^n \right) \gtrsim r(\delta + h).$$

¹An element is considered a neighbor if both share a vertex

²with r a small integer

For notational simplicity, the abbreviations $\mathcal{T}_r^n := \mathcal{T}_{r\delta, r+}^n$, $\mathcal{T}_r^{n, \mathcal{S}} := \mathcal{T}_{r\delta, r+}^{n, \mathcal{S}}$, $\mathcal{O}_r^n := \mathcal{O}_{r\delta, r+}^n$, $\mathcal{O}_r^{n, \mathcal{S}} := \mathcal{O}_{r\delta, r+}^{n, \mathcal{S}}$, and $\mathcal{V}_r^n := \mathcal{V}_{r\delta, r+}^n$ for $r \in \mathbb{N}$ will be frequently used below. We note that the introduced notation implies the following identities:

$$\begin{aligned} \Omega_h^n &= \Omega_\delta^n|_{\delta=0} = \Omega_0^n, & \mathcal{T}_\delta^n|_{\delta=0} &= \mathcal{T}_r^n|_{r=0} = \mathcal{T}_0^n, & \mathcal{O}_\delta^n|_{\delta=0} &= \mathcal{O}_r^n|_{r=0} = \mathcal{O}_0^n \\ \mathcal{T}_h^n &= \mathcal{T}_\delta^n|_{\delta \rightarrow \infty} = \mathcal{T}_\infty^n, & \mathcal{V}_h^n &= \mathcal{V}_\delta^n|_{\delta \rightarrow \infty} = \mathcal{V}_\infty^n \end{aligned}$$

Next, from \mathcal{F}_h^n , the set of all facets in the mesh \mathcal{T}_h^n , we introduce a set of *active facets* that is later on used for stabilization and extension purposes. To this end, we mark all facets between elements in the $r\delta$ strip and the interior:

$$(3.10) \quad \mathcal{F}_r^n := \{\bar{T}_1 \cap \bar{T}_2 \mid T_1 \in \mathcal{T}_r^n, T_2 \in \mathcal{T}_r^{n, \mathcal{S}}, T_1 \neq T_2\}.$$

Note that this selection of facets connects the domain interior of Ω_h^n with \mathcal{O}_r^n , i.e., the region obtained by applying an extension by $r\delta$ plus r additional element layers.

We further introduce a *patch* $\omega(\cdot) : \tilde{\Omega} \cup \mathcal{F}_h^n \cup \mathcal{T}_h^n \rightarrow \mathcal{T}_h^n$ that maps a point, a facet, or an element to a set of neighboring elements

$$(3.11a) \quad \omega(x) := \{\cup_{T \in \mathcal{T}_h^n} T, x \in \bar{T}\} \quad \text{for a point } x \in \tilde{\Omega},$$

$$(3.11b) \quad \omega(F) := \{\cup_{T \in \mathcal{T}_h^n} T, F \subset \bar{T}\} \quad \text{for a facet } F \in \mathcal{F}_h^n,$$

$$(3.11c) \quad \omega(T) := \{\cup_{T' \in \mathcal{T}_h^n} T' \mid \bar{T} \cap \bar{T}' \neq \emptyset\} \quad \text{for an element } T \in \mathcal{T}_h^n.$$

Similarly we use the notation $\hat{\omega}(\cdot)$ for patches on the undeformed mesh \mathcal{T}_h where the neighboring elements are picked correspondingly from \mathcal{T}_h .

We conclude this subsection with the following definition:

DEFINITION 3.2 (Trivial finite element extension). *We identify discrete functions on restricted meshes with functions on the whole mesh by setting all degrees of freedom outside the restriction to zero, s.t. there holds for instance $\mathcal{V}_\delta^n \subset \mathcal{V}_h^n$ for any $\delta \geq 0$.*

3.3. Properties of the parametric mapping as a function in space. Let $\phi(\mathbf{x}, t)$ be a given function which is smooth in space and Lipschitz-continuous in time at least in the vicinity of its zero level. The time-dependent mappings $\Theta^n : \tilde{\Omega} \rightarrow \tilde{\Omega}$ are constructed for each $n = 0, \dots, N$ based on the strategies for stationary domains described in [15, 20]. We only summarize the most important features. The mapping acts mainly on *cut elements*, i.e. on $\mathcal{O}_0^{n, \mathcal{S}}$, where the construction ensures that the image of the zero level of $\hat{\phi}_h^n$ under the mapping is (in a higher-order sense) close to the zero level of ϕ_h^n . Because the zero level of $\hat{\phi}_h^n$ is already exact on vertices and second order accurate elsewhere, the mapping is the identity on vertices and $\mathcal{O}(h^2)$ small on cut elements. On elements neighboring to cut elements, $\mathcal{O}_{0,+}^{n, \mathcal{S}} \setminus \mathcal{O}_0^{n, \mathcal{S}}$, a transition to the identity is realized so that overall the mapping Θ^n is small and local. By Ψ^n an *ideal* mapping is denoted that maps the zero level of $\hat{\phi}_h^n$ onto Γ^n exactly. As Θ^n the ideal mapping Ψ^n only deviates from the identity in $\mathcal{O}_{0,+}^{n, \mathcal{S}}$. Note that although not reflected in the notation Θ^n and Ψ^n depend on the triangulation \mathcal{T}_h .

We summarize the accuracy of the mapping in the following lemma:

LEMMA 3.3. *Let $n \in \{0, \dots, N\}$ be fixed and $\mathcal{O}_{0,+}^{n, \mathcal{S}}$ be the domain of cut elements*

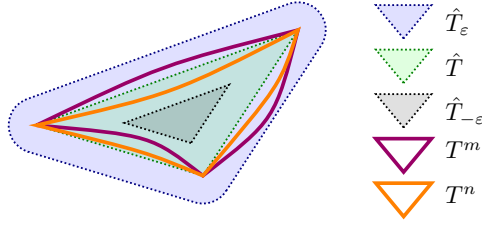


FIG. 3.2. Sketch of domains involved in Lemma 3.4.

and direct neighbors. For h sufficiently small, there holds

$$(3.12a) \quad \Theta^n(\mathbf{x}) = \mathbf{x}, \quad \text{for } \mathbf{x} = \mathbf{x}_V \text{ vertex in } \mathcal{T}_h \text{ or } \mathbf{x} \in \tilde{\Omega} \setminus \mathcal{O}_{0,+}^{n,S},$$

$$(3.12b) \quad \|\Theta^n - \text{id}\|_{\infty, \tilde{\Omega}} \lesssim h^2, \quad \|D\Theta^n(\mathbf{x}) - \mathbf{I}\|_{\infty, \tilde{\Omega}} \lesssim h,$$

$$(3.12c) \quad \|\Theta^n - \Psi^n\|_{\infty, \tilde{\Omega}} + h\|D(\Theta^n - \Psi^n)\|_{\infty, \tilde{\Omega}} \lesssim h^{q+1},$$

$$(3.12d) \quad \text{where the latter implies } \text{dist}(\partial\Omega(t), \partial\Omega_h(t)) \lesssim h^{q+1}.$$

Proof. See [20, Lemmas 3.4, 3.6 and 3.7]. \square

Next, we characterize inclusion relations between inflated and deflated elements:

LEMMA 3.4. Let $\hat{T} \in \mathcal{T}_h$, we define the (slightly) inflated version $\hat{T}_\varepsilon := \{x \in \tilde{\Omega} \mid \text{dist}(x, \partial\hat{T}) \leq \varepsilon\}$ ³ and the (slightly) deflated version $\hat{T}_{-\varepsilon} := \{x \in \hat{T} \mid \text{dist}(x, \partial\hat{T}) \geq \varepsilon\}$ for some $\varepsilon > 0$. Further, for $m = 0, \dots, N$, let $\Theta_T^{m*} : \hat{T}_\varepsilon \rightarrow \mathbb{R}^d$ denotes the canonical extension of the polynomial function $\Theta^m|_{\hat{T}}$ to \hat{T}_ε . For h sufficiently small there is $c_{L3.4} > 0$ (independent of h , \hat{T} and m , n) such that with $\varepsilon = c_{L3.4}h^2$ the following inclusion properties hold for $m, n = 0, \dots, N$ and $T_{\pm\varepsilon}^m := \Theta_T^{m*}(\hat{T}_{\pm\varepsilon})$, cf. Figure 3.2

$$(3.13) \quad T^n \subset \hat{T}_{\frac{\varepsilon}{2}} \subset T_\varepsilon^m, \quad \hat{T}_{-\varepsilon} \subset T^n \cap T^m \text{ with } \text{meas}_d\left((T^n \cup T^m) \setminus \hat{T}_{-\varepsilon}\right) \lesssim h^{d+1}.$$

Proof. Due to norm equivalences on the space of polynomials on a reference element and its extension, and standard scaling arguments, we have with $\varepsilon \simeq h^2 < 1$ that $\|\Theta_T^{m*} - \text{id}\|_{\infty, \hat{T}_\varepsilon} \lesssim \|\Theta^m|_{\hat{T}} - \text{id}\|_{\infty, \hat{T}} \lesssim h^2$ and $\|D\Theta_T^{m*} - \mathbf{I}\|_{\infty, \hat{T}_\varepsilon} \lesssim \|D\Theta^m|_{\hat{T}} - \mathbf{I}\|_{\infty, \hat{T}} \lesssim h$. Hence, the properties of (3.12b) carry over to the extended function Θ_T^{m*} which ensures the inclusion properties and the measure of the ε -band, i.e. $(T^n \cup T^m) \setminus \hat{T}_{-\varepsilon}$, with a bound εh^{d-1} where $\varepsilon \simeq h^2$. \square

A direct conclusion of the two previous lemmas and standard scaling arguments is that for $\hat{T} \in \mathcal{T}_h$, $T^n = \Theta_T^n(\hat{T})$ and $\hat{v} \in \mathcal{P}^k(\hat{T})$ there hold the following equivalences

$$(3.14) \quad \begin{aligned} h^{\frac{d}{2}} \|\hat{v} \circ \Theta_T^{-n}\|_{\mathcal{L}^\infty(T^n)} &\simeq \|\hat{v} \circ \Theta_T^{-n}\|_{T^n} \simeq \|\hat{v}\|_{\hat{T}} \simeq \|\hat{v}\|_{\mathcal{L}^\infty(\hat{T})} \\ &\quad \wr \quad \quad \quad \wr \quad \quad \quad \wr \quad \quad \quad \wr \\ h^{\frac{d}{2}} \|\hat{v} \circ \Theta_T^{-n}\|_{\mathcal{L}^\infty(T_{\pm\varepsilon}^n)} &\simeq \|\hat{v} \circ \Theta_T^{-n}\|_{T_{\pm\varepsilon}^n} \simeq \|\hat{v}\|_{\hat{T}_{\pm\varepsilon}} \simeq \|\hat{v}\|_{\mathcal{L}^\infty(\hat{T}_{\pm\varepsilon})}. \end{aligned}$$

3.4. Properties of the parametric mapping as a function in time. As mentioned above for the isoparametric approximation of the geometry we have slightly different meshes between consecutive time steps. To do proper time stepping in such an approach we need to project solutions from one deformed mesh to another. The details about this projection are discussed in the subsequent section. As such a

³Note that ε is not to be confused with ϵ introduced in Section 2 for the domain extension.

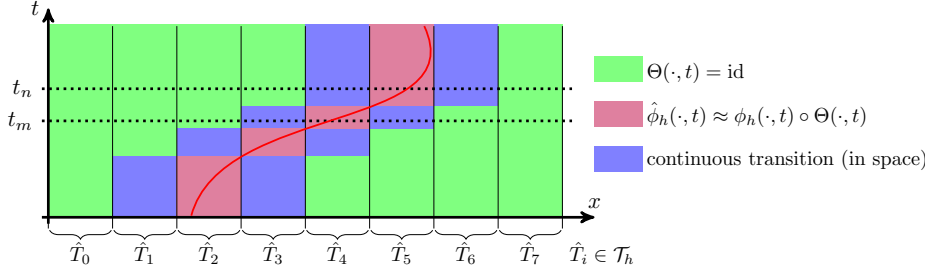


FIG. 3.3. Sketch of different regions for the mesh deformation. At a fixed time t an element is in exactly one of the three classes: cut (purple), transition (blue) or undeformed (green). Between two time instances $t_m < t_n$, for each fixed element we distinguish two situations: the type of the element and all its direct neighbors stay in the same class for all $t \in [t_m, t_n]$ or not.

projection has to be applied in every time step, one may expect projection errors accumulating with the number of time steps $N \sim \frac{1}{\Delta t}$. To be able to show (in the analysis section) that this is *not* the case we take a careful look at how the deformation depends on time. More specifically, we characterize where and when the deformation depends continuously on time and where and when not. This will then be exploited when analyzing the accumulation of the projection errors later in the analysis.

Based on the properties discussed above, for a fixed time t , there are three different types of deformed elements: cut elements, transition elements (neighboring to cut elements) and undeformed elements. The cut elements are transformed based on the desired property $\hat{\phi}_h(\cdot, t) \approx \phi_h(\cdot, t) \circ \Theta(\cdot, t)$, while the undeformed elements, sufficiently far away from cut elements, have $\Theta(\cdot, t) = \text{id}$. The remainder are transition elements which realize a proper blending between these two zones, cf. Figure 3.3 for a sketch in the spatially one-dimensional situation.

Now, we consider a fixed element $\hat{T} \in \mathcal{T}_h$ at two time instances $t_m < t_n$ and define a function (cut configuration changes) $\text{CCC} : \mathcal{T}_h \times [0, \mathbf{T}] \times [0, \mathbf{T}] \rightarrow \{\text{True}, \text{False}\}$ that allows to distinguish two cases:

- $\text{CCC}(\hat{T}, t_m, t_n) = \text{False}$: If \hat{T} and all direct neighbors stay in the same class of element types (uncut, transition, undeformed) then CCC evaluates to **False**. In this case the mesh deformation depends continuously on the change of the level set function which is assumed to change Lipschitz-continuously in time which yields the bound

$$(3.15a) \quad \|\Theta^m - \Theta^n\|_{\infty, \tilde{\Omega}} \leq |t_n - t_m|;$$

- $\text{CCC}(\hat{T}, t_m, t_n) = \text{True}$: If the type of element \hat{T} or one of its neighbors changes within the time interval $[t_m, t_n]$, then CCC evaluates to **True**. In this case the deformation on \hat{T} will not necessarily be Lipschitz-continuous in time. But due to Equation (3.12b) we still have that both Θ^m and Θ^n are close to the identity and hence

$$(3.15b) \quad \|\Theta^m - \Theta^n\|_{\infty, \tilde{\Omega}} \leq \|\Theta^m - \text{id}\|_{\infty, \tilde{\Omega}} + \|\text{id} - \Theta^n\|_{\infty, \tilde{\Omega}} \lesssim h^2.$$

Now let $t_i = i\Delta t$, $i = 1, \dots, N$ be the time steps of a partition in time. Then, for every fixed element $\hat{T} \in \mathcal{T}_h$ we define $N_D^T := \#\{i \in \{1, \dots, N\} \mid \text{CC}(\hat{T}, t_{i-1}, t_i) = \text{change}\}$ as the number of time steps for the case **change**, and $N_D = \max_{\hat{T} \in \mathcal{T}_h} \{N_D^T\}$ as the largest number of time steps among all \hat{T} for the case **change** with the mesh transformations *discontinuous* in time.

ASSUMPTION 1. *In the remainder we assume that for a fixed time interval $(0, \mathbf{T}]$ and a fixed computational mesh, the number N_D is bounded independent of the partition of time, but only depends on the motion of the domain.*

3.5. Transfer operator between meshes at different time steps. As mentioned above we have slightly different meshes between consecutive time steps. We therefore have to specify a transfer operator of finite element functions from one mesh to another. To this end, below in [Section 5](#) we design a projection operator $\Pi^n : \mathcal{V}_h^{n-1} \rightarrow \mathcal{V}_h^n$. We note that for locality and computational efficiency we choose a projection operator that deviates from a direct L^2 projection.

4. Definition of the stabilized Eulerian finite element method. Based on suitably adapted versions of the method of lines we introduce a full discretization. For ease of presentation we start with the low-order discretization in space and time, i.e., a piecewise linear finite element space with an implicit Euler time stepping in [Subsection 4.1](#). This allows us to present the spatial discretization with the involved stabilization and extension in its simplest configuration. The development to higher-order approximation in space is then tackled in [Subsection 4.2](#), which is followed by the extension also to higher-order approximation in time in [Subsection 4.3](#).

4.1. A fully discrete low order prototypical formulation. Let $k = q = 1$ in which case $\phi_h = \hat{\phi}_h$ and $\Theta^n = \text{id}$, $\mathcal{V}_h^n = \mathcal{V}_h$, $\mathcal{T}_h^n = \mathcal{T}_h$, $\Omega_h^n = \Omega_{\phi_h}^n$ for all $n = 0, \dots, N$. Each step in the low-order version as introduced in [\[17\]](#) consists of three parts: (i) the approximation of the partial time derivative through the finite difference stencil $\frac{u_h^n - u_h^{n-1}}{\Delta t}$; (ii) the spatially discrete operator b_h^n for convection and diffusion; (iii) a ghost-penalty-type operator s_r^n for extension and stabilization. The weak form reads: Find $u_h^n \in \mathcal{V}_1^n$, $n = 1, \dots, N$ for a given $u_h^0 \in \mathcal{V}_1^0$, such that

$$(4.1) \quad \int_{\Omega_h^n} \frac{u_h^n - u_h^{n-1}}{\Delta t} v_h \, dx + b_h^n(u_h^n, v_h) + \gamma s_1^n(u_h^n, v_h) = f_h^n(v_h), \quad \forall v_h \in \mathcal{V}_1^n.$$

Here, the bilinear form for convection and diffusion makes use of a skew-symmetrized form for the convection part

$$(4.2) \quad \begin{aligned} b_h^n(u_h, v_h) := & \int_{\Omega_h^n} \nu \nabla u_h \cdot \nabla v_h \, dx + \frac{1}{2} \int_{\Omega_h^n} ((\mathbf{w}^e \cdot \nabla u_h) v_h - (\mathbf{w}^e \cdot \nabla v_h) u_h) \, dx \\ & + \frac{1}{2} \int_{\Omega_h^n} (\nabla \cdot \mathbf{w}^e) u_h v_h \, dx + \frac{1}{2} \int_{\Gamma_h^n} (\mathbf{w}^e \cdot \mathbf{n}) u_h v_h \, ds, \quad \forall u_h, v_h \in \mathcal{H}^1(\Omega_h^n). \end{aligned}$$

where $(\cdot)^e$ denotes a smooth extension from Ω^n to Ω_h^n which we assume to exist.

The bilinear form $s_1^n(\cdot, \cdot)$ for extension and stabilization is applied with a parameter $\gamma(h, \delta)$, which is yet to be defined below. Here, this term uses the *ghost penalty* stabilization mechanism [\[1\]](#) where different versions to realize the same effect exists, cf. [\[17, Section 4.3\]](#). We make use of the *direct* or *volumetric jump* formulation introduced in [\[23\]](#) which takes the form (with $r = 1$ for the implicit Euler)

$$(4.3) \quad s_r^n(u_h, v_h) := \sum_{F^n \in \mathcal{F}^n} s_F^n(u_h, v_h) \text{ with } s_F^n(u_h, v_h) := \frac{1}{h^2} \int_{\omega(F^n)} (u_1 - u_2)(v_1 - v_2) dx,$$

where $\omega(F^n)$ is the patch of elements around F^n , cf. [Equation \(3.11b\)](#), and u_i, v_i , $i = 1, 2$ are canonical extensions of *mapped* polynomials, i.e. $u_i = (\mathcal{E}^{\mathcal{P}}(u_h|_{T_i^n} \circ \Theta_{T_i}^n)) \circ \Theta_{T_i}^{-n*}$

(and similarly for v_i) with $\Theta_{T_i}^{n*} = \mathcal{E}^{\mathcal{P}}(\Theta_{T_i}^n)$ where $\mathcal{E}^{\mathcal{P}} : \mathcal{P}_k(\hat{T}_i) \rightarrow \mathcal{P}_k(\mathbb{R}^d)$, $\hat{T}_i = \Theta_{T_i}^{-n}(T_i^n)$ is the canonical extension of a polynomial to the whole space⁴. The ghost penalty is responsible for two effects. On the one hand, it stabilizes the formulation to achieve robustness w.r.t. the position of the geometry within the elements. On the other hand, it implicitly realizes a discrete extension from Ω_h^n to $\mathcal{O}_1^n \supset \Omega_\delta^n$. This extension is required for instance to make u_h^n well-defined for the domain $\Omega_h^{n+1} \subset \Omega_\delta^n \subset \mathcal{O}_1^n$. To this end, we make the following assumption on δ :

$$(4.4) \quad \delta \geq \Delta t \|\mathbf{w}\|_{\mathcal{L}^\infty((0, \mathbf{T}), \mathcal{L}^\infty(\bar{\Omega}))}$$

Let us note that we take a global (in space and time) choice for δ to keep the presentation feasible, but a more localized definition of an extension region would easily be possible by considering different values for δ in different time steps and different spatial regions. Next, note that the solution is extended away from Ω_h^n by at least one layer of elements, i.e., by at least a distance proportional to h so that for a constant $c > 0$, depending only on the shape regularity there holds

$$(4.5) \quad \text{dist}(\partial\mathcal{O}_1^n, \partial\Omega_h^n) \geq \delta + ch \gtrsim \Delta t + h.$$

With $\Omega_h^{n+1} \subset \Omega^n$ and $\text{dist}(\partial\Omega_h^n, \partial\Omega^n) \lesssim h^2$ for all $n = 0, \dots, N$ we can guarantee the inclusion $\Omega_h^{n+1} \subset \Omega_\delta^n \subset \mathcal{O}_1^n$ (for sufficiently small h). The linear functional f_h^n is simply $f_h^n(v_h) := \int_{\Omega_h^n} g v_h dx$ for $v_h \in \mathcal{H}^1(\Omega_h^n)$. If the time step is bounded by

$$(4.6) \quad \Delta t < \xi^{-1} := 2 \left(\|\text{div}(\mathbf{w}^e)\|_{\mathcal{L}^\infty(\Omega_h^n)} + \nu + c_{\Omega_h}^2 \|\mathbf{w}^e \cdot \mathbf{n}\|_{\mathcal{L}^\infty(\Omega_h^n)} / 4\nu \right)^{-1},$$

where c_{Ω_h} is the constant of the multiplicative trace inequality, b_h^n has a lower bound

$$(4.7) \quad b_h^n(v, v) \geq \frac{\nu}{2} \|\nabla v\|_{\Omega_h^n}^2 - \xi \|v\|_{\Omega_h^n}^2.$$

Here we assume that the (extended) velocity \mathbf{w}^e has bounded divergence and normal flux. For details cf. [17, Lemma 3.1 and Remark 4.1]. The coercivity of the overall l.h.s. bilinear form on \mathcal{V}_1^n w.r.t. the norm

$$(4.8) \quad \|v\|_n := \left(\frac{\nu}{2} \|\nabla v\|_{\Omega_h^n}^2 + \|v\|_{\Omega_h^n}^2 + \gamma s_r^n(v, v) \right)^{\frac{1}{2}}$$

guarantees the unique solvability based on the Lax-Milgram theorem.

Before specifying the parameter γ we introduce the following assumption.

ASSUMPTION 2. *Let $\mathcal{T}_r^{n, \mathcal{S}^+}$ denote the subset of $\mathcal{T}_r^{n, \mathcal{S}}$ where for at least one point $\mathbf{x} \in T$ there holds $\phi_h(\mathbf{x}) > 0$. To every element in $\mathcal{T}_r^{n, \mathcal{S}^+}$ we require an element in $\mathcal{T}_r^n \setminus \mathcal{T}_r^{n, \mathcal{S}^+}$ that can be reached by repeatedly passing through facets in \mathcal{F}_r^n . We assume that the number of facets passed through during this path is bounded by $K \lesssim (1 + \frac{\delta}{h})$. Further, every ‘‘interior’’ element in the active domain, i.e. $T \in \mathcal{T}_r^n \setminus \mathcal{T}_r^{n, \mathcal{S}^+}$, provides at most M paths in which it serves as the terminal element of such paths, where M is a number that is bounded independently of h and Δt .*

With this definition of K , we specify – following [17, Section 4.4] – $\gamma(h, \delta) = c_\gamma K \lesssim 1 + \delta/h$ for a constant c_γ independent of Δt and h . This complete the fully discrete low-order scheme.

⁴Note that $u_h|_{T_i^n}$, $i = 1, 2$ are only mapped polynomials but $u_h|_{T_1^n} \circ \Theta_{T_1}^n$ are standard ones.

4.2. Higher order space discretization. The discretization above can be advanced trivially to higher order in space if we assume exact geometry handling or sufficiently accurate quadrature on $\Omega_{\phi_h}^n$ as given. As the former is typically not realistic and the latter is hard to guarantee, we consider the application of the isoparametric mapping Θ^n to achieve higher order of geometrical accuracy. However, with the time-dependent deformation of the mesh, which implies $\mathcal{T}_h^{n-1} \neq \mathcal{T}_h^n$ and hence $u_h^{n-1} \notin \mathcal{V}_h^n$, the need to apply a few adaptations arises. We make use of the *consecutive* transfer operator $\Pi^n : \mathcal{V}_h^{n-1} \rightarrow \mathcal{V}_h^n$, introduced in more detail in [Subsection 5.1](#), to project initial data u_h^{n-1} from one timestep to the next, and then the weak form reads: Find $u_h^n \in \mathcal{V}_1^n$, $n = 1, \dots, N$ for a given $u_h^0 \in \mathcal{V}_1^0$, such that

$$(4.9) \quad \int_{\Omega_h^n} \frac{u_h^n - \Pi^n u_h^{n-1}}{\Delta t} v_h \, dx + b_h^n(u_h^n, v_h) + \gamma s_1^n(u_h^n, v_h) = f_h^n(v_h), \quad \forall v_h \in \mathcal{V}_1^n.$$

4.3. High order time discretization based on BDF schemes. For high order approximation in time we apply BDF schemes to the time derivative. We introduce the notation $\partial_{\Delta t}^r(\dots)$ for the BDF time stencils (for $r = 1, 2, 3$):

$$(4.10a) \quad \partial_{\Delta t}(u_h^n, u_h^{n-1}) := \frac{u_h^n - u_h^{n-1}}{\Delta t}, \quad r = 1;$$

$$(4.10b) \quad \partial_{\Delta t}^2(u_h^n, u_h^{n-1}, u_h^{n-2}) := \frac{3u_h^n - 4u_h^{n-1} + u_h^{n-2}}{2\Delta t}, \quad r = 2;$$

$$(4.10c) \quad \partial_{\Delta t}^3(u_h^n, u_h^{n-1}, u_h^{n-2}, u_h^{n-3}) := \frac{11u_h^n - 18u_h^{n-1} + 9u_h^{n-2} - 2u_h^{n-3}}{6\Delta t}, \quad r = 3.$$

In order to apply the stencils we need to take advantage of the projection operator. To do this across several time steps we define the consecutive application of projection operators over all intermediate time steps

$$(4.11) \quad \Pi_{n-r}^n : \mathcal{V}_h^{n-r} \rightarrow \mathcal{V}_h^n, \quad v \mapsto \Pi^n \Pi^{n-1} \dots \Pi^{n-r+1} v.$$

Then, the weak form reads:

Find $u_h^n \in \mathcal{V}_r^n$, $n = r, \dots, N$ for given $u_h^0 \in \mathcal{V}_r^0, \dots, u_h^{r-1} \in \mathcal{V}_r^{r-1}$, such that for $\forall v_h \in \mathcal{V}_r^n$

$$(4.12) \quad \int_{\Omega_h^n} \partial_{\Delta t}^r(u_h^n, \dots, \Pi_{n-r}^n u_h^{n-r}) v_h \, dx + b_h^n(u_h^n, v_h) + \gamma s_r^n(u_h^n, v_h) = f_h^n(v_h).$$

Note that the stabilization bilinear form s_r^n now expands to a larger region extended by $r\delta$ distance plus r additional element layers.

Remark 4.1. In an implementation it is not necessary to apply the whole chain of the projection Π_{n-l}^n for $1 < l \leq r$ as the terms involving Π^m , $m < n$ will be needed in previous time steps already and can be reused, i.e., there is actually only the projection Π^n to be evaluated at each time step (on possibly several terms though).

5. Efficient higher-order projection for isoparametric unfitted FEM.

In this section we discuss the operator Π^n between consecutive time levels in detail.

5.1. Definition of a projection based on essentially local operations.

Let $v_{\mathcal{T}_h^m} \in \mathcal{V}_h^m$, $m = n - 1$ be a discrete function⁵ w.r.t. to the mesh \mathcal{T}_h^m . We aim to approximate it on \mathcal{T}_h^n with $v_{\mathcal{T}_h^n} := \Pi_m^n v_{\mathcal{T}_h^m} \in \mathcal{V}_h^n$, i.e., a discrete function w.r.t. to the (slightly different) mesh \mathcal{T}_h^n . This projection is achieved in three steps:

⁵Remember that we identify functions on restricted domain, e.g., in $\mathcal{V}_{h,\delta}^m$ with their finite element extensions by setting the remaining degrees of freedom to zero.

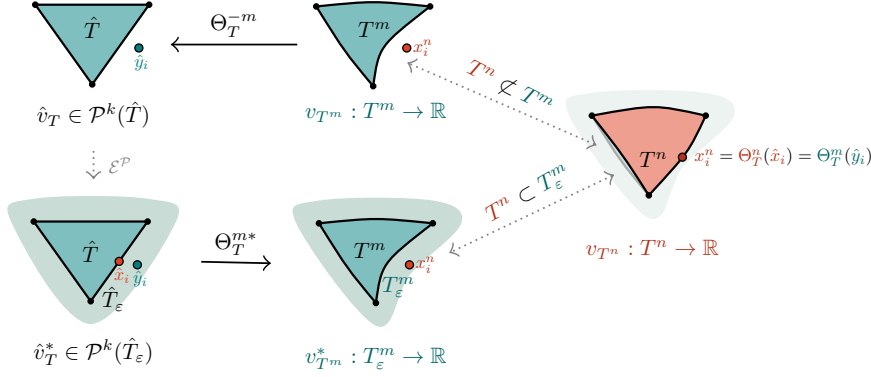


FIG. 5.1. Sketch of extension (Subsection 5.1.1) and transfer operation (Subsection 5.1.2). For an element $T^m = \Theta_T^m(\hat{T}) \in \mathcal{T}_h^m$ the extension T_ε^m covers $T^n = \Theta_T^n(\hat{T}) \in \mathcal{T}_h^n$. For a Lagrange node x_i^n in T^n the mappings Θ_T^{-n} and Θ_T^{-m*} , respectively, yield different points \hat{x}_i, \hat{y}_i in \hat{T}_ε .

- (i) Firstly, by exploiting that $v_{T^m} := v_{\mathcal{T}_h^m}|_{T^m}$, the restriction of $v_{\mathcal{T}_h^m}$ to an element $T^m \in \mathcal{T}_h^m$, is smooth, we define an extension $v_{T^m}^*$ of v_{T^m} to a small neighborhood T_ε^m of T^m with $T^n \subset T_\varepsilon^m$, such that $v_{T^m}^* \in \mathcal{C}^\infty(T_\varepsilon^m)$;
- (ii) Secondly, we project these extensions into $\bigoplus_{T^n \in \mathcal{T}_h^n} \mathcal{V}_h^n|_{T^n}$, i.e., the discontinuous (across element interfaces) version of \mathcal{V}_h^n , yielding $\tilde{v}_{\mathcal{T}_h^n}$;
- (iii) Thirdly, we apply an Oswald-type interpolation of $\tilde{v}_{\mathcal{T}_h^n}$ to obtain $v_{\mathcal{T}_h^n} \in \mathcal{V}_h^n$.

The first two steps are completely element-local and allow for a trivial parallelization, especially as the access to neighboring elements is not necessary, whereas the third step is a very efficient vector operation (averaging). This is in contrast to an only seemingly simpler approach such as a global \mathcal{L}^2 projection.

5.1.1. Element-local extensions. For an undeformed element $\hat{T} \in \mathcal{T}_h$ we introduce the notation $T^i = \Theta_T^i(\hat{T}) \in \mathcal{T}_h^i$ with $\Theta_T^i := \Theta^i|_{\hat{T}} \in [\mathcal{P}^q(\hat{T})]^d$, $i \in \{m, n\}$.

The restriction of $v_{\mathcal{T}_h^m} \in \mathcal{V}_h^m$ to T^m , i.e. $v_{T^m} := v_{\mathcal{T}_h^m}|_{T^m}$, is a mapped polynomial. We can map it back to the undeformed element $\hat{T} \in \mathcal{T}_h$ and realize that there is $\hat{v}_T \in \mathcal{P}^k(\hat{T})$ such that $v_{T^m} = \hat{v}_T \circ \Theta_T^{-m}$. Let $\hat{v}_T^* = \mathcal{E}^{\mathcal{P}} \hat{v}_T \in \mathcal{P}^k(\hat{T}_\varepsilon)$ and $\Theta_T^{m*} = \mathcal{E}^{\mathcal{P}} \Theta_T^m \in [\mathcal{P}^q(\hat{T}_\varepsilon)]^d$ be the canonical extension of this polynomial to the ε -neighborhood \hat{T}_ε of \hat{T} . With $v_{T^m}^* := \hat{v}_T^* \circ \Theta_T^{-m*} = \mathcal{E}^{\mathcal{P}} \hat{v}_T \circ (\mathcal{E}^{\mathcal{P}} \Theta_T^m)^{-1}$ we have a smooth extension of v_{T^m} from T^m to $T_\varepsilon^m := \Theta_T^{m*}(\hat{T}_\varepsilon)$, such that $v_{T^m}^*|_{T^m} = v_{T^m}$ still holds and furthermore $T^n \subset T_\varepsilon^m$. A sketch of this extension is given in Figure 5.1.

5.1.2. Element-local interpolation (shifted evaluation). With $T^n \subset T_\varepsilon^m$, we can define the following element-local interpolation that for given $v_{T^m}^*$ as constructed in the previous section it yields $\tilde{v}_{T^n} \in \mathcal{P}^k(\hat{T}) \circ \Theta_T^{-n}$, or equivalently $\hat{v}_{T^n} \in \mathcal{P}^k(\hat{T})$ with $\hat{v}_{T^n} = \tilde{v}_{T^n} \circ \Theta_T^n$, by nodal interpolation.

Let $L(\hat{T}) = \{\hat{x}_i\}_{i=1, \dots, M_L}$, $M_L = \#L(\hat{T})$ be the set of Lagrange nodes of $\mathcal{V}_h^n|_{\hat{T}} = \mathcal{P}^k(\hat{T})$ on \hat{T} with corresponding set of Lagrange basis functions $\{\hat{\varphi}_i\}_{i=1, \dots, M_L}$, s.t. $\hat{\varphi}_i(\hat{x}_j) = \delta_{ij}$, $i, j = 1, \dots, M_L$. The correspondingly mapped nodes and basis functions are $L(T^n) := \{x_i^n\}_{i=1, \dots, M_L}$ and $\{\varphi_i^n\}_{i=1, \dots, M_L}$ with $x_i^n = \Theta_T^n(\hat{x}_i)$ and $\varphi_i^n = \hat{\varphi}_i \circ \Theta_T^{-n}$. We define

$$(5.1a) \quad \tilde{v}_{T^n}(x) := \sum_{i=1}^{M_L} v_{T^m}^*(x_i^n) \varphi_i^n(x), \quad \forall x \in T^n$$

or equivalently, with $v_{T^m}^* = \hat{v}_T^* \circ \Theta_T^{-m*}$ and $x_i^n = \Theta_T^n(\hat{x}_i)$ we have

$$(5.1b) \quad \hat{v}_T(\hat{x}) := \sum_{i=1}^{M_L} \hat{v}_T^* \left(\underbrace{\Theta_T^{-m*}(\Theta_T^n(\hat{x}_i))}_{\hat{y}_i} \right) \hat{\varphi}_i(\hat{x}), \quad \forall \hat{x} \in \hat{T}.$$

Let us stress that $\hat{x}_i \neq \hat{y}_i := \Theta_T^{-m*}(x_i^n)$ and we hence call this step *shifted evaluation*, cf. [Figure 5.1](#) for a sketch of the relation between \hat{x}_i and \hat{y}_i . By setting $\tilde{v}_{\mathcal{T}_h^n}|_{T^n} := \tilde{v}_{T^n}$ for all $T^n \in \mathcal{T}_h^n$ we obtain $\tilde{v}_{\mathcal{T}_h^n} \in \bigoplus_{T^n \in \mathcal{T}_h^n} \mathcal{V}_h^n|_{T^n}$.

5.1.3. Projection into the space of continuous functions. After the previous steps we obtain a discontinuous, element-wise (mapped) polynomial approximation on \mathcal{T}_h^n . We then apply an Oswald-type quasi-interpolation $P_h : \bigoplus_{T^n \in \mathcal{T}_h^n} C(T^n) \rightarrow \mathcal{V}_h^n$ in order to get a continuous function in \mathcal{V}_h^n . Let $L(\mathcal{T}_h^n) = \{x_i^n\}$ be the set of Lagrange nodes of \mathcal{V}_h^n on \mathcal{T}_h^n , and $\{\varphi_i^n\}$ the set of corresponding Lagrange basis functions. Let $\omega(x_i^n)$ be the set of elements containing the Lagrange node x_i^n . The Oswald-type projector P_h is the following generalization of the Lagrange interpolation for a discontinuous function v :

$$(5.2) \quad P_h v := \sum_{x_i^n \in L(\mathcal{T}_h^n)} \left(\#\omega(x_i^n)^{-1} \sum_{T^n \in \omega(x_i^n)} v|_{T^n}(x_i^n) \right) \varphi_i^n.$$

5.2. Analysis of the projection. We start with a simple observation for the norm evaluation w.r.t. one mesh of a function defined on another (slightly different) mesh.

LEMMA 5.1. *For $v_h \in \mathcal{V}_h^n$, $w_h \in \mathcal{V}_h^m$, $T_i = \Theta_T^i(\hat{T})$, $\hat{T} \in \mathcal{T}_h$, $i \in \{m, n\}$, there holds*

$$(5.3) \quad \|v_h + w_h\|_{T^n} \lesssim h^{\frac{d}{2}} \|v_h + w_h\|_{\mathcal{L}^\infty(T_{-\varepsilon}^n)} + h^{\frac{5}{2}} \|\nabla v_h\|_{T^n} + h^{\frac{5}{2}} \|\nabla w_h\|_{\omega(T^m)}.$$

Proof. Obviously we have $\|v_h + w_h\|_{T^n} \lesssim \|v_h + w_h\|_{T_{-\varepsilon}^n} + \|v_h + w_h\|_{T^n \setminus T_{-\varepsilon}^n}$. The first term on the right hand side is simply bounded by $h^{\frac{d}{2}} \|v_h + w_h\|_{\mathcal{L}^\infty(T_{-\varepsilon}^n)}$. For the second term we use [Lemma 3.4](#), i.e. $\text{meas}_d(T^n \setminus T_{-\varepsilon}^n) \lesssim h^{d+1}$, and that for $x \in T^n \setminus T_{-\varepsilon}^n$ there is $y \in \partial T_{-\varepsilon}^n$ and $z \in \text{conv}\{x, y\} \subset T \setminus T_{-\varepsilon}^n$ such that $|(v_h + w_h)(x)| \leq |(v_h + w_h)(y)| + |(\nabla(v_h + w_h))(z)| |y - x|$, and hence with $\varepsilon \lesssim h^2$ we obtain

$$\begin{aligned} \|v_h + w_h\|_{T^n \setminus T_{-\varepsilon}^n} &\lesssim h^{\frac{d+1}{2}} \|v_h + w_h\|_{\mathcal{L}^\infty(T^n \setminus T_{-\varepsilon}^n)} \\ &\lesssim h^{\frac{d+1}{2}} \left(\|v_h + w_h\|_{\mathcal{L}^\infty(T_{-\varepsilon}^n)} + \varepsilon \|\nabla(v_h + w_h)\|_{\mathcal{L}^\infty(T^n \setminus T_{-\varepsilon}^n)} \right) \\ &\lesssim h^{\frac{d+1}{2}} \left(\|v_h + w_h\|_{\mathcal{L}^\infty(T_{-\varepsilon}^n)} + h^2 \|\nabla v_h\|_{\mathcal{L}^\infty(T^n)} + h^2 \|\nabla w_h\|_{\mathcal{L}^\infty(\omega(T^m))} \right) \\ &\lesssim h^{\frac{d+1}{2}} \|v_h + w_h\|_{\mathcal{L}^\infty(T_{-\varepsilon}^n)} + h^{\frac{5}{2}} \|\nabla v_h\|_{T^n} + h^{\frac{5}{2}} \|\nabla w_h\|_{\omega(T^m)}. \end{aligned}$$

For the last step we made use of norm equivalences on a reference element after transformation⁶. \square

LEMMA 5.2. *Let $\Pi^n : \mathcal{V}_h^m \rightarrow \mathcal{V}_h^n$, $m = n - 1$ be the projection for a discrete function $v_h \in \mathcal{V}_h^m$ from the mesh \mathcal{T}_h^m to the mesh \mathcal{T}_h^n . Further, let $\tilde{\mathcal{T}}_h \subset \mathcal{T}_h$ be*

⁶Note that we cannot directly apply such a result for $v_h + w_h$ as w_h and v_h are not from the same (mapped) polynomial space.

an arbitrary selection of elements and the corresponding deformed meshes $\tilde{\mathcal{T}}_h^m, \tilde{\mathcal{T}}_h^n$ with the corresponding domains $\tilde{\mathcal{O}}_h^m, \tilde{\mathcal{O}}_h^n$, respectively. For $c_{5.2a} > 0$ and $c_{5.2b} > 0$ independent of h and Δt there holds for $\hat{T} \in \mathcal{T}_h$, $T^n = \Theta_T^n(\hat{T})$, $T^m = \Theta_T^m(\hat{T})$:

$$(5.4a) \quad \|\Pi^n v_h\|_{T^n}^2 \lesssim \|v_h\|_{\omega(T^m)}^2, \quad \|\Pi^n v_h\|_{\tilde{\mathcal{O}}_h^n}^2 \leq c_{5.2a} \|v_h\|_{\tilde{\mathcal{O}}_{h,+}^m}^2,$$

$$(5.4b) \quad \|\nabla \Pi^n v_h\|_{T^n}^2 \lesssim \|\nabla v_h\|_{\omega(T^m)}^2, \quad \|\nabla \Pi^n v_h\|_{\tilde{\mathcal{O}}_h^n}^2 \leq c_{5.2b} \|\nabla v_h\|_{\tilde{\mathcal{O}}_{h,+}^m}^2.$$

Proof. We have $\|\Pi^n v_h\|_{T^n} \simeq \|\Pi^n v_h\|_{T_{-\varepsilon}^n}$, cf. (3.14). For $x \in T_{-\varepsilon}^n$ and $\hat{x} = \Theta^{-n}(x) \in \hat{T}_{-\varepsilon}$ we have by definition (recall the notation introduced in Subsection 5.1)

$$\Pi^n v_h(x) = \sum_{i=1}^{M_L} \left(\#\hat{\omega}(x_i^n)^{-1} \sum_{\tilde{T} \in \hat{\omega}(x_i^n)} \hat{v}_{\tilde{T}}^*(\hat{y}_i) \right) \hat{\varphi}_i(\hat{x})$$

for $M_L = \#L(T^n) \lesssim 1$ the number of Lagrange nodes on T^n and the patch w.r.t. to the undeformed mesh \mathcal{T}_h , $\hat{\omega}(x_i^n) = \Theta^{-m}(\omega(x_i^n))$. Hence $\|\Pi^n v_h\|_{T_{-\varepsilon}^n} \lesssim h^{\frac{d}{2}} \|v_h\|_{\mathcal{L}^\infty(\omega(T^m))} \lesssim \|v_h\|_{\omega(T^m)}$. Summing over all elements in $\tilde{\mathcal{T}}_h^n$ yields the first result. For the second equation we proceed similarly after introducing $\bar{v}_h = \frac{1}{|\omega(T^m)|} \int_{\omega(T^m)} v_h ds$ with $\Pi^n \bar{v}_h = \bar{v}_h$ on $T_{-\varepsilon}^n$

$$\begin{aligned} \|\nabla \Pi^n v_h\|_{T_{-\varepsilon}^n} &= \|\nabla \Pi^n (v_h - \bar{v}_h)\|_{T_{-\varepsilon}^n} \lesssim h^{\frac{d}{2}} h^{-1} \|v_h - \bar{v}_h\|_{\mathcal{L}^\infty(\omega(T^m))} \\ &\lesssim h^{-1} \|v_h - \bar{v}_h\|_{\omega(T^m)} \lesssim \|\nabla v_h\|_{\omega(T^m)}. \quad \square \end{aligned}$$

LEMMA 5.3. *Let $\Pi^n : \mathcal{V}_h^m \rightarrow \mathcal{V}_h^n$, $m = n - 1$ be the projection for a discrete function $v_h \in \mathcal{V}_h^m$ from the mesh \mathcal{T}_h^m to the mesh \mathcal{T}_h^n . Then there holds for $T^n \in \mathcal{T}_h^n$ and $T^m = \Theta^m(\Theta^{-n}(T^n)) \in \mathcal{T}_h^m$*

$$(5.5a) \quad \|(\text{id} - \Pi^n)v_h\|_{T^n} \lesssim h^2 \|\nabla v_h\|_{\omega(T^m)} \lesssim h \|v_h\|_{\omega(T^m)}.$$

Here, $\omega(T^m)$ is the element patch to T^m . Hence for an arbitrary selection of elements $\tilde{\mathcal{T}}_h$ and the corresponding deformed meshes $\tilde{\mathcal{T}}_h^m, \tilde{\mathcal{T}}_h^n$ with the corresponding domains $\tilde{\mathcal{O}}_h^m, \tilde{\mathcal{O}}_h^n$, respectively, there holds

$$(5.5b) \quad \|(\text{id} - \Pi^n)v_h\|_{\tilde{\mathcal{O}}_h^n} \lesssim h^2 \|\nabla v_h\|_{\tilde{\mathcal{O}}_{h,+}^m} \lesssim h \|v_h\|_{\tilde{\mathcal{O}}_{h,+}^m}.$$

Proof. Let $T^n = \Theta_T^n(\hat{T}) \in \mathcal{T}_h^n$, $T^m = \Theta_T^m(\hat{T}) \in \mathcal{T}_h^m$ for $\hat{T} \in \mathcal{T}_h$. With Lemma 5.1 and Lemma 5.2 we have

$$\|(\text{id} - \Pi^n)v_h\|_{T^n} \lesssim h^{\frac{d}{2}} \|(\text{id} - \Pi^n)v_h\|_{\mathcal{L}^\infty(T_{-\varepsilon}^n)} + h^{\frac{5}{2}} \|\nabla v_h\|_{\omega(T^m)}.$$

We start with bounding the \mathcal{L}^∞ norm. For $\forall x \in T_{-\varepsilon}^n \subset T^n \cap T^m$ and $\hat{x} := \Theta_T^{-n}(x)$, we have by definition

$$(v_h - \Pi^n v_h)(x) = \sum_{i=1}^{M_L} \left(\#\hat{\omega}(x_i^n)^{-1} \sum_{\tilde{T} \in \hat{\omega}(x_i^n)} (\hat{v}_{\tilde{T}}^*(\hat{x}_i) - \hat{v}_{\tilde{T}}^*(\hat{y}_i)) \right) \hat{\varphi}_i(\hat{x})$$

for $M_L = \#L(T^n) \lesssim 1$ the number of Lagrange nodes on T^n and the element patch w.r.t. the undeformed mesh $\hat{\omega}(x_i^n) = \Theta^{-m}(\omega(T^m)) \subset \mathcal{T}_h$. With the second-order

boundedness of Θ^i , $i \in \{m, n\}$, cf. [Lemma 3.3](#), we have $|\hat{x}_i - \hat{y}_i| \lesssim h^2$ and hence for every \hat{T} in the element patch $\hat{\omega}(\hat{T})$ there holds

$$|\hat{v}_{\hat{T}}^*(\hat{x}_i) - \hat{v}_{\hat{T}}^*(\hat{y}_i)| \lesssim h^2 \|\nabla \hat{v}_{\hat{T}}^*\|_{\mathcal{L}^\infty(\hat{T}_\varepsilon)} \lesssim h^2 \|\nabla \hat{v}_{\hat{T}}\|_{\mathcal{L}^\infty(\hat{T})} \lesssim h^{2-\frac{d}{2}} \|\nabla \hat{v}_{\hat{T}}\|_{\hat{T}}.$$

Here, we made use of the norm equivalence on finite dimensional spaces and scaling arguments. This yields [\(5.5a\)](#). Summing over \hat{T}_h^n we obtain [\(5.5b\)](#) by using finite overlap. \square

LEMMA 5.4. *Let $\Pi^n : \mathcal{V}_h^m \rightarrow \mathcal{V}_h^n$, $m = n - 1$ be the projection for a discrete function $v_h \in \mathcal{V}_h^m$ from the mesh \mathcal{T}_h^m to the mesh \mathcal{T}_h^n . For constants $c_{5.4a}$ and $c_{5.4b}$ independent of h and Δt there holds*

$$(5.6) \quad s_1^n(\Pi^n v_h, \Pi^n v_h) \leq c_{5.4a} s_2^m(v_h, v_h) + c_{5.4b} h^2 \|\nabla v_h\|_{\mathcal{O}_{h,2}^{n-1,S}}^2.$$

Proof (sketch). The proof relies on the application of an estimate of triangle inequality type for each involved facet, $s_F^n(\Pi^n v_h, \Pi^n v_h) \lesssim s_F^m(v_h, v_h) + \|\Pi^n v_h - v_h\|_{\omega(F)}^2$, and the estimates from [Lemma 5.3](#). The details are technical and given only in the appendix for completeness, cf. [Appendix A](#). \square

The previous lemmas describe "the worst case" scenarios as v_h is allowed to be arbitrarily rough in \mathcal{V}_h^m . Assuming more smoothness helps to improve the bound.

LEMMA 5.5. *Let $\Pi^n : \mathcal{V}_h^m \rightarrow \mathcal{V}_h^n$, $m = n - 1$ be the projection for a discrete function $v_h \in \mathcal{V}_h^m$ from the mesh \mathcal{T}_h^m to the mesh \mathcal{T}_h^n . For any $\hat{T} \in \mathcal{T}_h$ and $T^n = \Theta^n(\hat{T}) \in \mathcal{T}_h^n$, $v \in \mathcal{W}_\infty^{k+1}(T_\varepsilon^n) \cap C^0(\omega(T^n))$ and \mathcal{I}_h^p the Lagrange interpolation w.r.t. \mathcal{T}_h^p , $p \in \{m, n\}$, there holds*

$$(5.7) \quad \|(\mathcal{I}_h^n - \Pi^n \mathcal{I}_h^m)v\|_{T^n} \lesssim \|\Theta^n - \Theta^m\|_{\mathcal{L}^\infty(\hat{\omega}(\hat{T}))} h^{k+\frac{d}{2}} |v|_{\mathcal{W}_\infty^{k+1}(T_\varepsilon^n)}.$$

Proof. Let $\varphi_i^p := \hat{\varphi}_i \circ \Theta_T^{-p}$ be the Lagrange basis functions of $\mathcal{V}_h^p|_{T^p}$ w.r.t. the Lagrange nodes $x_i^p := \Theta_T^p(\hat{x}_i)$ on $T^p \in \mathcal{T}_h^p$ such that $\varphi_i^p(x_j^p) = \delta_{ij}$, $i, j = 1, \dots, M_L := \#L(T^p)$. Analogously to the local interpolation operator $\mathcal{I}_{T^p}^p$ on T^p we define the nodal interpolation operator on the extension T_ε^p of T^p , i.e. for $p \in \{m, n\}$ such that

$$\mathcal{I}_{T^p}^p v(x) := \sum_{i=1}^{M_L} v(x_i^p) \varphi_i^p(x), \quad \text{and} \quad \mathcal{I}_{T_\varepsilon^p}^p v(x) := \sum_{i=1}^{M_L} v(x_i^p) \varphi_i^{p*}(x), \quad v \in \mathcal{L}^\infty(T^p),$$

where $(\cdot)^* = \mathcal{E}^p \cdot$ canonically extends the basis functions φ_i^p on $T^p \in \mathcal{T}_h^p$ to T_ε^p . With the definition of the projection Π^n , cf. [Subsection 5.1](#), we have for $x \in T^n$

$$(\mathcal{I}_h^n v - \Pi^n \mathcal{I}_h^m v)(x) = \sum_{j=1}^{M_L} \left(\#\omega(x_j^m)^{-1} \sum_{\hat{T}^m \in \omega(x_j^m)} \left((v - \mathcal{I}_{\hat{T}_\varepsilon^m}^m v)(x_j^m) \right) \right) \varphi_j^n(x)$$

for any $v \in C^0(\omega(T^m))$. Taking the \mathcal{L}^2 -norm on $T^n \in \mathcal{T}_h^n$ then this yields

$$(5.8) \quad \|\mathcal{I}_h^n v - \Pi^n \mathcal{I}_h^m v\|_{T^n} \lesssim h^{\frac{d}{2}} \max_{\hat{T}^m \in \omega(T^m)} \left\| v - \mathcal{I}_{\hat{T}_\varepsilon^m}^m v \right\|_{l_\infty(L(T^n))}$$

where we made use of $\|\sum_{j=1}^{M_L} \varphi_j^n\|_{T^n} \lesssim h^{\frac{d}{2}}$. Let the Taylor polynomial of degree k that expands a function \hat{v} at node \hat{x}_j^m be denoted by $\hat{\mathfrak{T}}_{\hat{x}_j^m}$. We introduce the mapped

Taylor polynomial (to the element \tilde{T} in the patch $\omega(T^m)$) by transformation to the straight element applying the Taylor expansion there and transforming back, i.e., as $\mathfrak{T}_{x_j^m} v := \left(\hat{\mathfrak{T}}_{\hat{x}_j^m} (v \circ \Theta_{\tilde{T}}^{m*}) \right) \circ \Theta_{\tilde{T}}^{-m*}$ such that there holds $\mathfrak{T}_{x_j^m} v = \mathcal{I}_{\tilde{T}_\varepsilon^m}^m \mathfrak{T}_{x_j^m} v$. For $j = 1, \dots, M_L$ we then have

$$(5.9) \quad \begin{aligned} \left| (v - \mathcal{I}_{\tilde{T}_\varepsilon^m}^m v)(x_j^n) \right| &= \left| (v - \mathfrak{T}_{x_j^m} v)(x_j^n) + (\mathfrak{T}_{x_j^m} v - \mathcal{I}_{\tilde{T}_\varepsilon^m}^m v)(x_j^n) \right| \\ &\leq \left| (v - \mathfrak{T}_{x_j^m} v)(x_j^n) \right| + \left| \mathcal{I}_{\tilde{T}_\varepsilon^m}^m (\mathfrak{T}_{x_j^m} v - v)(x_j^n) \right| \end{aligned}$$

For the first part we simply have with $x_j^n = \Theta_{\tilde{T}}^n(\hat{x}_j)$, $x_j^m = \Theta_{\tilde{T}}^m(\hat{x}_j)$ and $x_j^n, x_j^m \in T_\varepsilon^n$:

$$\left| (v - \mathfrak{T}_{x_j^m} v)(x_j^n) \right| \lesssim |x_j^n - x_j^m|^{k+1} |v|_{\mathcal{W}_\infty^{k+1}(T_\varepsilon^n)} \lesssim \|\Theta_{\tilde{T}}^n - \Theta_{\tilde{T}}^m\|_{\mathcal{L}^\infty(\hat{T})}^{k+1} |v|_{\mathcal{W}_\infty^{k+1}(T_\varepsilon^n)}.$$

For the second part we exploit $(\mathfrak{T}_{x_j^m} v - v)(x_j^m) = 0$ to obtain

$$\begin{aligned} \left| \mathcal{I}_{\tilde{T}_\varepsilon^m}^m (\mathfrak{T}_{x_j^m} v - v)(x_j^n) \right| &= \left| \sum_{i=1}^{M_L} (\mathfrak{T}_{x_j^m} v - v)(x_i^m) \varphi_i^{m*}(x_j^n) \right| = \left| \sum_{i \neq j} (\mathfrak{T}_{x_j^m} v - v)(x_i^m) \varphi_i^{m*}(x_j^n) \right| \\ &\lesssim \max_{i \neq j} |\varphi_i^{m*}(x_j^n)| \max_{i \neq j} |(\mathfrak{T}_{x_j^m} v - v)(x_i^m)| \lesssim \max_{i \neq j} |\varphi_i^{m*}(x_j^n)| \underbrace{|x_i^m - x_j^m|^{k+1}}_{\lesssim h^{k+1}} |v|_{\mathcal{W}_\infty^{k+1}(T_\varepsilon^n)}. \end{aligned}$$

Finally we bound $|\varphi_i^{m*}(x_j^n)|$ for $i \neq j$ by using $\varphi_i^{m*}(x_j^m) = 0$: $\lesssim h^{k+1}$ ■

$$|\varphi_i^{m*}(x_j^n)| = |\varphi_i^{m*}(x_j^n) - \varphi_i^{m*}(x_j^m)| \lesssim \|\nabla \varphi_i^{m*}\|_{\mathcal{L}^\infty(\hat{T}_\varepsilon)} \|x_j^n - x_j^m\| \lesssim h^{-1} \|\Theta_{\tilde{T}}^n - \Theta_{\tilde{T}}^m\|_{\mathcal{L}^\infty(\hat{T})}$$

Altogether, by summing over all \tilde{T}^m in $\omega(T^m)$ we obtain the claim (5.7). \square

6. A priori error analysis. The analysis follows a similar strategy as in [17] and where possible, we will refer to the corresponding results. In the analysis of the method we will only treat the case of a BDF2 discretization, i.e., we fix $r = 2$. Necessary changes compared to [17] occur due to the projection Π_m^n and the second-order time difference stencil $\partial_{\Delta t}^2$, c.f. Subsection 4.3. To deal with the BDF2 scheme in the following stability analysis we define a suitable norm and make a simple but useful observation, cf. [5, Lemma 6.33].

LEMMA 6.1. *Let $u_h, v_h, w_h \in \mathcal{V}_{h,2}^n$. For $S \subseteq \mathcal{O}_2^n$ we define the BDF2 tuple norm*

$$(6.1) \quad \|(w_h, v_h)\|_S^2 := \|w_h\|_S^2 + \|2w_h - v_h\|_S^2,$$

so that for $\partial_{\Delta t}^2$ as in (4.10b) there holds

$$(6.2) \quad (4\Delta t \partial_{\Delta t}^2 (w_h, v_h, u_h), w_h)_{\Omega_h^n} \geq \|(w_h, v_h)\|_{\Omega_h^n}^2 - \|(v_h, u_h)\|_{\Omega_h^n}^2.$$

Proof. Multiplying the terms out we find, cf. [5, Lemma 6.33]:

$$\begin{aligned} (4\Delta t \partial_{\Delta t}^2 (w_h, v_h, u_h), w_h)_{\Omega_h^n} &= \|w_h\|_{\Omega_h^n}^2 + \|2w_h - v_h\|_{\Omega_h^n}^2 \\ &\quad - \|v_h\|_{\Omega_h^n}^2 - \|2v_h - u_h\|_{\Omega_h^n}^2 + \underbrace{\|w_h - 2v_h + u_h\|_{\Omega_h^n}^2}_{\geq 0}. \quad \square \end{aligned}$$

Let us note that similar norms with a corresponding estimate can also be defined for BDF3 and BDF4, cf. [21, Section 2]. Similarly, the analysis below can also be transferred to $r = 3$ and $r = 4$. We however decided to treat only the case $r = 2$ to keep the technicalities at a manageable level.

As a consequence of the errors introduced by the mesh transfer operator, in the subsequent analysis, we make the following assumption on the ratio between space and time refinements.

ASSUMPTION 3. We assume that as h and Δt go to zero, $\frac{h^4}{\Delta t}$ converges to zero too. Then, for any constant $c_{A3} > 0$ there is an $h_0 > 0$ so that for all meshes with mesh size $h < h_0$ we have $\frac{h^4}{\nu \Delta t} < c_{A3}$.

Remark 6.2. Assumption 3 is only a restriction on the efficiency for very high order in space. Assuming an $\mathcal{L}^2(0, \mathbf{T}; \mathcal{H}^1(\Omega))$ -error bound of the form⁷ $\mathcal{O}(\Delta t^2 + h^k)$. Only for $k \geq 8$ a scaling $h \geq \Delta t^{\frac{1}{4}}$ would be beneficial for the efficiency of the scheme.

We will need certain space-time norms, which we will abbreviate, e.g., $\mathcal{L}^\infty(\mathcal{H}^k)$ for $\mathcal{L}^\infty(0, \mathbf{T}; \mathcal{H}^k(\Omega(t)))$ and $\mathcal{L}^\infty(\mathcal{W}_\infty^k)$ for $\mathcal{L}^\infty(0, \mathbf{T}; \mathcal{W}_\infty^k(\Omega(t)))$.

Furthermore, in the remainder we treat the asymptotic behavior, $h, \Delta t \rightarrow 0$ only, i.e., we implicitly assume h and Δt sufficiently small at several occasions.

6.1. Error splitting and error equation. Let u be the exact solution to (2.1). For $u^n := u(t_n)$, $n = 0, 1, \dots, N$, we make use of the extension operator $\mathcal{E} : \mathcal{L}^2(\Omega^n) \rightarrow \mathcal{L}^2(\Omega_\epsilon^n)$ introduced in [17, Section 3.2.1]. $\mathcal{E}u^n$ is well-defined on $\Omega_\epsilon^n \supset \Omega^{n+r}$ and \mathcal{E} is uniformly continuous in standard Sobolev norms. In the following we assume that ϵ can be chosen sufficiently large so that $\Omega_\epsilon^n \supset \mathcal{O}_r^n$ and identify $\mathcal{E}u^n$ with u^n .

First, we introduce an error splitting. We define $u_I^n := \mathcal{I}_h^n u^n \in \mathcal{V}_h^n$ the global Lagrange interpolant w.r.t. to \mathcal{T}_h^n such that the error can be split into

$$(6.3) \quad \mathbf{e}^n := u^n - u_h^n = \mathbf{e}_I^n + \mathbf{e}_h^n, \quad \mathbf{e}_I^n := u^n - u_I^n, \quad \mathbf{e}_h^n := u_I^n - u_h^n,$$

for the approximation error \mathbf{e}_I^n and the discrete error \mathbf{e}_h^n , respectively. In addition, we split the approximation error after mesh transfer between \mathcal{V}_h^m and \mathcal{V}_h^n :

$$(6.4) \quad \tilde{\mathbf{e}}^m := u^m - \Pi_m^n u_h^m = \tilde{\mathbf{e}}_I^m + \Pi_m^n \mathbf{e}_h^m, \quad \tilde{\mathbf{e}}_I^m := u^m - \Pi_m^n u_I^m.$$

Here, $\tilde{\mathbf{e}}_I^m$ is the corresponding approximation error after projection, and $\Pi_m^n \mathbf{e}_h^m$ is the projection of the corresponding discrete error.

We then introduce a lifting operator $(\cdot)^\ell : \mathcal{H}^1(\Omega_h^n) \rightarrow \mathcal{H}^1(\Omega^n)$, $v_h \mapsto v_h \circ \Theta \circ \Psi^{-1}$, and $b^n(\cdot, \cdot)$, $f^n(\cdot)$ as the bilinear and linear forms $b_h^n(\cdot, \cdot)$, $f_h^n(\cdot)$ with Ω_h^n , Γ_h^n replaced by Ω^n , Γ^n . For the exact solution to (2.1) there holds

$$\int_{\Omega^n} \partial_t u^n \tilde{v}_h \, dx + b^n(u^n, \tilde{v}_h) = f^n(\tilde{v}_h) \quad \forall \tilde{v}_h \in \mathcal{H}^1(\Omega^n),$$

from which we subtract (4.12) to obtain the error equation

$$(6.5) \quad \int_{\Omega_h^n} \partial_{\Delta t}^2(\mathbf{e}^n, \tilde{\mathbf{e}}^{n-1}, \tilde{\mathbf{e}}^{n-2}) v_h \, dx + b_h^n(\mathbf{e}^n, v_h) + \gamma s_r^n(\mathbf{e}^n, v_h) = \mathbf{E}_C^n(v_h)$$

with the consistency error term that we decompose into four contributions

$$(6.6) \quad \mathbf{E}_C^n(v_h) := \overbrace{\int_{\Omega_h^n} \partial_{\Delta t}^2(u^n, u^{n-1}, u^{n-2}) v_h \, dx}^{\mathbf{E}_C^{n,1}(v_h)} - \int_{\Omega^n} \partial_t u^n v_h^\ell \, dx \\ + \underbrace{b_h^n(u^n, v_h) - b^n(u^n, v_h^\ell)}_{\mathbf{E}_C^{n,2}(v_h)} + \underbrace{\gamma s_r^n(u^n, v_h)}_{\mathbf{E}_C^{n,3}(v_h)} + \underbrace{f^n(v_h^\ell) - f_h^n(v_h)}_{\mathbf{E}_C^{n,4}(v_h)}.$$

⁷see also the numerical examples for a motivation of this ansatz

Further splitting \mathbf{e}^n and $\tilde{\mathbf{e}}^{n-1}, \tilde{\mathbf{e}}^{n-2}$ in the error equation yields

$$(6.7) \quad \int_{\Omega_h^n} \partial_{\Delta t}^2(\mathbf{e}_h^n, \Pi^n \mathbf{e}_h^{n-1}, \Pi_{n-2}^n \mathbf{e}_h^{n-2}) v_h dx + b_h^n(\mathbf{e}_h^n, v_h) + \gamma s_r^n(\mathbf{e}_h^n, v_h) = \mathbf{E}_C^n(v_h) + \mathbf{E}_I^n(v_h)$$

with the interpolation error term

$$(6.8) \quad \mathbf{E}_I^n(v_h) := - \underbrace{\int_{\Omega_h^n} \partial_{\Delta t}^2(\mathbf{e}_I^n, \tilde{\mathbf{e}}_I^{n-1}, \tilde{\mathbf{e}}_I^{n-2}) v_h dx}_{\mathbf{E}_I^{n,1}(v_h)} - \underbrace{b_h^n(\mathbf{e}_I^n, v_h) + \gamma s_r^n(\mathbf{e}_I^n, v_h)}_{\mathbf{E}_I^{n,2}(v_h)}.$$

6.2. Consistency and approximation bounds.

LEMMA 6.3. *Let $u \in \mathcal{L}^\infty(\mathcal{H}^{k+1})$ with $\partial_t^3 u \in \mathcal{L}^\infty(Q)$ be the exact solution to (2.1) and let $g \in \mathcal{L}^\infty(\mathcal{W}_\infty^1)$, then the consistency error in (6.6) has the following bound for all $v_h \in \mathcal{V}_h^n$:*

$$|\mathbf{E}_C^n(v_h)| \lesssim \left(\Delta t^2 + h^q + h^k K^{\frac{1}{2}} \right) \mathcal{R}_{6.3} \|v_h\|_n$$

with $\mathcal{R}_{6.3} = \mathcal{R}_{6.3}(u, g) := \|\partial_t^3 u\|_{\mathcal{L}^\infty(Q)} + \|u\|_{\mathcal{L}^\infty(\mathcal{H}^{k+1})} + \|g\|_{\mathcal{L}^\infty(\mathcal{W}_\infty^1)}$. Here, we recall the semi-norm $\|v_h\|_n^2 = \|v_h\|_{\Omega_h^n}^2 + \frac{\nu}{2} \|\nabla v_h\|_{\Omega_h^n}^2 + \gamma s_2^n(v_h, v_h)$.

Proof (sketch). The proof follows along the lines of the proof of [17, Lemma 5.11] and for completeness is given in the appendix, cf. Appendix A. \square

LEMMA 6.4. *For any $u \in \mathcal{L}^\infty(\mathcal{W}_\infty^{k+1})$ with $\partial_t u \in \mathcal{L}^\infty(\mathcal{H}^k)$, the interpolation errors in (6.8) have the following bound for all $v_h \in \mathcal{V}_h^n$:*

$$(6.9) \quad \sum_{n=2}^N |\mathbf{E}_I^{n,1}(v_h)| \lesssim N^{\frac{1}{2}} h^k \mathcal{R}_{6.4} \|v_h\|_{l_2}, \quad |\mathbf{E}_I^{n,2}(v_h)| \lesssim K^{\frac{1}{2}} h^k \|u\|_{\mathcal{H}^{k+1}(\Omega_h^n)} \|v_h\|_n$$

with $\mathcal{R}_{6.4} = \mathcal{R}_{6.4}(u) := \|\partial_t u\|_{\mathcal{L}^\infty(\mathcal{H}^k)} + \|u\|_{\mathcal{L}^\infty(\mathcal{W}_\infty^{k+1})}$ and $\|v_h\|_{l_2}^2 := \sum_{n=2}^N \|v_h\|_{\Omega_h^n}^2$. Here, we recall the semi-norm $\|v_h\|_n^2 = \|v_h\|_{\Omega_h^n}^2 + \frac{\nu}{2} \|\nabla v_h\|_{\Omega_h^n}^2 + \gamma s_2^n(v_h, v_h)$.

Proof. We start with the first term $\mathbf{E}_I^{n,1}(v_h)$ in (6.8) and sum it over all time steps from $n = 2$ to N . Let $T_\Omega^n := T^n \cap \Omega_h^n$, then with Cauchy-Schwarz we obtain

$$\begin{aligned} \sum_{n=2}^N |\mathbf{E}_I^{n,1}(v_h)| &= \sum_{n=2}^N \left| \int_{\Omega_h^n} \underbrace{\partial_{\Delta t}^2(\mathbf{e}_I^n, \tilde{\mathbf{e}}_I^{n-1}, \tilde{\mathbf{e}}_I^{n-2})}_{=: z^n} v_h dx \right| \leq \sum_{T^n \in \mathcal{T}_h^n} \sum_{n=2}^N \int_{T_\Omega^n} |z^n| |v_h| dx \\ &\leq \sum_{T^n \in \mathcal{T}_h^n} \sum_{n=2}^N \|z^n\|_{T_\Omega^n} \|v_h\|_{T_\Omega^n} \leq \sum_{T \in \mathcal{T}_h^n} \left(\sum_{n=2}^N \|z^n\|_{T_\Omega^n}^2 \right)^{\frac{1}{2}} \left(\sum_{n=2}^N \|v_h\|_{T_\Omega^n}^2 \right)^{\frac{1}{2}} \end{aligned}$$

Another triangle inequality yields the splitting

$$\begin{aligned} \sum_{n=2}^N \|z^n\|_{T_\Omega^n}^2 &\leq \sum_{n=2}^N \left\| \frac{3\mathbf{e}_I^n - 4\tilde{\mathbf{e}}_I^{n-1} + \tilde{\mathbf{e}}_I^{n-2}}{2\Delta t} \right\|_{T_\Omega^n}^2 \lesssim \underbrace{\Delta t^{-2} \sum_{n=2}^N \left\| 3\mathbf{e}_I^n - 4\tilde{\mathbf{e}}_I^{n-1} + \tilde{\mathbf{e}}_I^{n-2} \right\|_{T_\Omega^n}^2}_{=: Z_1} \\ &\quad + \underbrace{\Delta t^{-2} \sum_{n=2}^N \left\| 4(\mathcal{I}_h^n - \Pi^n \mathcal{I}_h^{n-1})u^{n-1} - (\mathcal{I}_h^n - \Pi_{n-2}^n \mathcal{I}_h^{n-2})u^{n-2} \right\|_{T_\Omega^n}^2}_{=: Z_2}. \end{aligned}$$

With $\mathbf{e}_I(t) := u(t) - \mathcal{I}_h u(t)$, the first part Z_1 can easily be estimated as follows

$$Z_1 = \Delta t^{-2} \sum_{n=2}^N \left\| 3 \int_{t_{n-1}}^{t_n} \partial_t \mathbf{e}_I(t) dt - \int_{t_{n-2}}^{t_{n-1}} \partial_t \mathbf{e}_I(t) dt \right\|_{T_\Omega^n}^2 \lesssim N h^{2k} \|\partial_t u\|_{\mathcal{L}^\infty(\mathcal{H}^k)(T_\Omega^n)}^2$$

For the second part Z_2 we split the expression into the two parts

$$\Delta t^2 Z_2 \leq \underbrace{\sum_{n=2}^N \left\| (\mathcal{I}_h^n - \Pi^n \mathcal{I}_h^{n-1})(4u^{n-1} - u^{n-2}) \right\|_{T_\Omega^n}^2}_{=:\Delta t^2 Z_2^a} + \underbrace{\sum_{n=2}^N \left\| \Pi^n (\mathcal{I}_h^{n-1} - \Pi^{n-1} \mathcal{I}_h^{n-2}) u^{n-2} \right\|_{T_\Omega^n}^2}_{=:\Delta t^2 Z_2^b}$$

We start with Z_2^a and apply [Lemma 5.5](#):

$$\begin{aligned} Z_2^a &\lesssim \Delta t^{-2} \sum_{n=2}^N \left\| (\mathcal{I}_h^n - \Pi^n \mathcal{I}_h^{n-1})(4u^{n-1} - u^{n-2}) \right\|_{T_\Omega^n}^2 \\ &\lesssim \Delta t^{-2} \sum_{n=2}^N \|\Theta^n - \Theta^{n-1}\|_{\mathcal{L}^\infty(\hat{\omega}(\hat{T}))}^2 h^{2k+d} \|4u^{n-1} - u^{n-2}\|_{\mathcal{W}_\infty^{k+1}(T_\varepsilon^n)}^2 \\ &\lesssim (N + N_D \Delta t^{-2} h^4) h^{2k+d} \sup_{n=1, \dots, N} \|u\|_{\mathcal{W}_\infty^{k+1}(T_\varepsilon^n)}^2 \end{aligned}$$

where we recall that by [Assumption 1](#) for most of the time steps there is $\|\Theta^n - \Theta^m\|_\infty \lesssim \Delta t$, while for a bounded number of time steps N_D there is $\|\Theta^n - \Theta^m\|_\infty \lesssim h^2$. For Z_2^b we additionally make use of [\(5.4a\)](#) which extends the relevant region by one element layer yielding

$$Z_2^b \lesssim (N + N_D \Delta t^{-2} h^4) h^{2k+d} \sup_{t \in [0, \mathbf{T}]} \|u\|_{\mathcal{W}_\infty^{k+1}(\omega(T^n) \star \cap \Omega_\varepsilon^n)}^2$$

As a consequence, with $N_D \lesssim N \Delta t$ and $\frac{h^4}{\Delta t} \lesssim 1$, cf. [Assumption 3](#), we arrive at $(N + N_D \Delta t^{-2} h^4) \lesssim N$ and hence, after summing over the mesh, the bound

$$\sum_{T^n \in \mathcal{T}_h^n} \sum_{n=2}^N \|z\|_{T_\Omega^n}^2 \lesssim N h^{2k} \left(\|\partial_t u\|_{\mathcal{L}^\infty(\mathcal{H}^{k+1})}^2 + \underbrace{(\#\mathcal{T}_h^n) h^d}_{\lesssim 1} \|u\|_{\mathcal{L}^\infty(\mathcal{W}_\infty^{k+1})}^2 \right).$$

Next, we estimate the second term $\mathbf{E}_I^{n,2}(v_h)$ in [\(6.8\)](#) (as in [\[17, Lemma 5.12\]](#)) with Cauchy-Schwarz inequality and interpolation estimates, i.e.

$$\begin{aligned} |b_h^n(\mathbf{e}_I^n, v_h)| &\leq \|\mathbf{e}_I^n\|_{\mathcal{H}^1(\Omega^n)} \|v_h\|_{\mathcal{H}^1(\Omega_h^n)} \lesssim h^k \|u^n\|_{\mathcal{H}^{k+1}(\Omega^n)} (\|v_h\|_{\Omega_h^n} + \frac{\nu}{2} \|\nabla v_h\|_{\Omega_h^n}), \\ \gamma s_2^n(\mathbf{e}_I^n, v_h) &\leq \gamma s_2^n(\mathbf{e}_I^n, \mathbf{e}_I^n)^{\frac{1}{2}} s_2^n(v_h, v_h)^{\frac{1}{2}} \lesssim K^{\frac{1}{2}} h^k \|u^n\|_{\mathcal{H}^{k+1}(\Omega^n)} (\gamma s_2^n(v_h, v_h))^{\frac{1}{2}}. \end{aligned}$$

Hence, we obtain the following bound for $\mathbf{E}_I^{n,2}(v_h)$:

$$|\mathbf{E}_I^{n,2}(v_h)| \lesssim (1 + K^{\frac{1}{2}}) h^k \|u^n\|_{\mathcal{H}^{k+1}(\Omega^n)} (\|v_h\|_{\Omega_h^n} + \frac{\nu}{2} \|\nabla v_h\|_{\Omega_h^n} + \gamma s_2^n(v_h, v_h)^{\frac{1}{2}}).$$

This concludes the proof. \square

6.3. The ghost penalty mechanism. We introduce a slight generalization of an important result [17] concerning the bound of the extensions obtained through the application of the ghost penalties.

LEMMA 6.5. *For $v_h \in \mathcal{V}_r^n$, $r \in \{1, 2, 3\}$ and for all $\theta > 0$ there holds*

$$(6.10a) \quad \|v_h\|_{\mathcal{O}_r^n}^2 \lesssim \|v_h\|_{\Omega_h^n}^2 + Kh^2 s_r^n(v_h, v_h)$$

$$(6.10b) \quad \|\nabla v_h\|_{\mathcal{O}_r^n}^2 \lesssim \|\nabla v_h\|_{\Omega_h^n}^2 + K s_r^n(v_h, v_h)$$

$$(6.10c) \quad \|v_h\|_{\mathcal{O}_r^n}^2 \leq (1 + c_{6.5a}\Delta t)\|v_h\|_{\Omega_h^n}^2 + c_{6.5b}\nu\Delta t\|\nabla v_h\|_{\Omega_h^n}^2 + c_{6.5c}\Delta t K s_r^n(v_h, v_h)$$

with constants $c_{6.5a} = c_{6.5}r(1+\theta^{-1})$, $c_{6.5b}(\theta) = c_{6.5}r\theta\nu^{-1}$, $c_{6.5c} = c_{6.5}r(\theta+h^2+h^2\theta^{-1})$ for a constant $c_{6.5} > 0$ independent of h and Δt .

Proof. The proof follows from [17, Lemma 5.2, Lemma 5.5 and Lemma 5.7] with minor modification for an extended strip size from \mathcal{O}_δ^n (in [17]) to \mathcal{O}_r^n (here). \square

Note that the constant $c_{6.5b}$ can be decreased at the price of an increase of $c_{6.5a}$ by choosing θ accordingly. We will make use of this later in order to drive $c_{6.5b}$ sufficiently small. In the following we will however only reflect that dependency on θ for $c_{6.5b}$.

Next, we bound the BDF2 tuple norm of a tuple of functions transferred from Ω_h^{n-1} and Ω_h^{n-2} to Ω_h^n .

LEMMA 6.6. *For any $c_{6.6b} > 0$ there holds for sufficiently small h that for all $w_h \in \mathcal{V}_2^{n-1}$ and $v_h \in \mathcal{V}_2^{n-2}$*

$$\begin{aligned} & \|(\Pi^n w_h, \Pi^n \Pi^{n-1} v_h)\|_{\Omega_h^n}^2 \leq (1 + c_{6.6a}\Delta t)\|(w_h, \Pi^{n-1} v_h)\|_{\Omega_h^{n-1}}^2 \\ & + c_{6.6b}\nu\Delta t\{\|\nabla w_h\|_{\Omega_h^{n-1}}^2 + \|\nabla v_h\|_{\Omega_h^{n-2}}^2\} + c_{6.6c}K\Delta t\{s_1^{n-1}(w_h, w_h) + s_2^{n-2}(v_h, v_h)\} \end{aligned}$$

for constants $c_{6.6a}$, $c_{6.6c}$ that are independent of h , Δt or n .

Proof. Using (6.1) to unroll the BDF2 norm, together with a triangle inequality and Lemma 5.3 on each part separately yields

$$\|(\Pi^n w_h, \Pi^n \Pi^{n-1} v_h)\|_{\Omega_h^n}^2 \leq \|(w_h, \Pi^{n-1} v_h)\|_{\Omega_h^n}^2 + c_{(5.5b)}h^4\|(\nabla w_h, \nabla \Pi^{n-1} v_h)\|_{\mathcal{O}_1^{n-1}}^2.$$

To go from Ω_h^n to Ω_h^{n-1} for the first part on the r.h.s. we exploit $\Omega_h^n \subset \mathcal{O}_1^{n-1}$ and apply (6.10c) from Lemma 6.5 with $r = 1$:

$$\begin{aligned} \|(\Pi^n w_h, \Pi^n \Pi^{n-1} v_h)\|_{\Omega_h^n}^2 & \leq (1 + c_{6.5a}\Delta t)\|(w_h, \Pi^{n-1} v_h)\|_{\Omega_h^{n-1}}^2 \\ & + (c_{6.5b}\nu\Delta t + c_{(5.5b)}h^4)\|(\nabla w_h, \nabla \Pi^{n-1} v_h)\|_{\mathcal{O}_1^{n-1}}^2 \\ & + c_{6.5c}\Delta t(8K s_1^{n-1}(w_h, w_h) + 2K s_1^{n-1}(\Pi^{n-1} v_h, \Pi^{n-1} v_h)) \end{aligned}$$

In the last step we used $s_1^{n-1}(2a-b, 2a-b) \leq 8s_1^{n-1}(a, a) + 2s_1^{n-1}(b, b)$ for $a, b \in \mathcal{V}_2^{n-1}$. The first part on the r.h.s. is already in the desired form with $c_{6.6a} := c_{6.5a}$. We hence continue with the second part. After splitting the terms in the BDF2 norm, we use (5.4b) to bound $\|\nabla \Pi^{n-1} v_h\|_{\mathcal{O}_1^{n-1}}^2$ with $\|\nabla v_h\|_{\mathcal{O}_2^{n-2}}^2$, and (6.10b) from Lemma 6.5

$$\begin{aligned} & \|(\nabla w_h, \nabla \Pi^{n-1} v_h)\|_{\mathcal{O}_1^{n-1}}^2 \leq 9\|\nabla w_h\|_{\mathcal{O}_1^{n-1}}^2 + 2\|\nabla \Pi^{n-1} v_h\|_{\mathcal{O}_1^{n-1}}^2 \\ & \leq 9\|\nabla w_h\|_{\mathcal{O}_1^{n-1}}^2 + 2c_{(5.4b)}c_{(6.10b)}(\|\nabla v_h\|_{\Omega_h^{n-2}}^2 + K s_2^{n-2}(v_h, v_h)) \\ & \leq 9c_{(6.10b)}(\|\nabla w_h\|_{\Omega_h^{n-1}}^2 + K s_1^{n-1}(w_h, w_h)) + 2c_{(5.4b)}c_{(6.10b)}(\|\nabla v_h\|_{\Omega_h^{n-2}}^2 + K s_2^{n-2}(v_h, v_h)). \end{aligned}$$

Finally, it only remains to bound the ghost penalty stabilization term on $\Pi^{n-1}v_h$. We use Lemma 5.4 and (6.10b) from Lemma 6.5, so that

$$\begin{aligned} s_1^{n-1}(\Pi^{n-1}v_h, \Pi^{n-1}v_h) &\leq c_{5.4a}s_2^{n-2}(v_h, v_h) + c_{5.4b}h^2\|\nabla v_h\|_{\mathcal{O}_2^{n-2}}^2 \\ &\leq (c_{5.4a} + c_{5.4b}c_{(6.10b)})h^2Ks_2^{n-2}(v_h, v_h) + c_{5.4b}c_{(6.10b)}h^2\|\nabla v_h\|_{\Omega_h^{n-2}}^2. \end{aligned}$$

Now, we need to collect all pieces together. Ensured by Assumption 3 we can bound $(c_{6.5b}\nu\Delta t + c_{(5.5b)}h^4) \leq 2c_{6.5b}\nu\Delta t$ and obtain the conditions

$$\begin{aligned} \max\{18c_{6.5b}c_{(6.10b)}, 4c_{5.4b}c_{6.5b} + 2c_{6.5c}c_{6.5b}c_{5.4b}c_{(6.10b)}K/\nu h^2\} &\leq c_{6.6b}, \\ \max\{18c_{6.5b}c_{(6.10b)}\nu + 8c_{6.5c}, 4c_{6.5b}c_{5.4b}c_{(6.10b)}\nu + 4c_{6.5c}(c_{5.4a} + c_{5.4b}c_{(6.10b)})h^2K\} &\leq c_{6.6c}. \end{aligned}$$

We note that the latest terms in the max can always be neglected for sufficiently small h . In the remaining terms only $c_{6.5b}$ and $c_{6.5c}$ depend on the choice of θ in Lemma 6.5. Hence, for every choice of $c_{6.6b}$ we can choose θ and $c_{6.6c}$ to meet the claim. \square

6.4. Stability analysis.

THEOREM 6.7. *The solution $\{u_h^n\}$ of (4.12) with $r = 2$ satisfies the stability bound*

$$\begin{aligned} \|(u_h^N, \Pi^N u_h^{N-1})\|_{\Omega_h^N}^2 + \Delta t \sum_{n=2}^N (\nu \|\nabla u_h^n\|_{\Omega_h^n}^2 + 2\gamma s_2^n(u_h^n, u_h^n)) &\lesssim \exp(c_{6.7}t_N) R^0 \text{ with} \\ R^0 := \|(u_h^1, \Pi^1 u_h^0)\|_{\Omega_h^1}^2 + \Delta t \left(\sum_{n=2}^N \|g^n\|_{\Omega_h^n}^2 + \sum_{n=0}^1 (\nu \|\nabla u_h^n\|_{\Omega_h^n}^2 + K s_2^n(u_h^n, u_h^n)) \right), \end{aligned}$$

for $c_{6.7} := c_{6.6a} + \frac{1}{2} + 4\xi$ with ξ as in (4.6), i.e. independent of \mathbf{T} , h or Δt .

Proof. We test (4.12) with $v_h = 4\Delta t u_h^n$ and apply (6.2) which yields

$$\begin{aligned} \|(u_h^n, \Pi^n u_h^{n-1})\|_{\Omega_h^n}^2 + 4\Delta t b_h^n(u_h^n, u_h^n) + 4\Delta t \gamma s_2^n(u_h^n, u_h^n) \\ (6.11) \quad \leq \|(\Pi^n u_h^{n-1}, \Pi^n \Pi^{n-1} u_h^{n-2})\|_{\Omega_h^n}^2 + 4\Delta t f_h^n(u_h^n). \end{aligned}$$

Recall the lower bound of $b_h^n(\cdot, \cdot)$ from (4.7). We apply Lemma 6.6 on the r.h.s. followed by Young's inequality with $\beta > 0$ and Cauchy-Schwartz applied to f_h^n :

$$\begin{aligned} (1 - 4\Delta t \xi) \|(u_h^n, \Pi^n u_h^{n-1})\|_{\Omega_h^n}^2 + 2\Delta t \nu \|\nabla u_h^n\|_{\Omega_h^n}^2 + 4\Delta t \gamma s_2^n(u_h^n, u_h^n) \\ \leq (1 + c_{6.6a}\Delta t) \|(u_h^{n-1}, \Pi^{n-1} u_h^{n-2})\|_{\Omega_h^{n-1}}^2 + c_{6.6b}\nu\Delta t (\|\nabla u_h^{n-1}\|_{\Omega_h^{n-1}}^2 + \|\nabla u_h^{n-2}\|_{\Omega_h^{n-2}}^2) \\ + c_{6.6c}\Delta t (K s_2^{n-1}(u_h^{n-1}, u_h^{n-1}) + K s_2^{n-2}(u_h^{n-2}, u_h^{n-2})) + 2\Delta t (\beta^{-1} \|g^n\|_{\Omega_h^n}^2 + \beta \|u_h^n\|_{\Omega_h^n}^2). \end{aligned}$$

Summing over $n = 2, \dots, N \leq N$, choosing $c_{6.6b} \leq \frac{1}{2}$, and assuming $\gamma \geq c_{6.6c}K$ yields

$$\begin{aligned} (1 - 4\Delta t \xi - 2\Delta t \beta) \|(u_h^N, \Pi^N u_h^{N-1})\|_{\Omega_h^N}^2 + \Delta t \sum_{n=2}^N \nu \|\nabla u_h^n\|_{\Omega_h^n}^2 + 2\Delta t \sum_{n=2}^N \gamma s_2^n(u_h^n, u_h^n) \\ (6.12) \quad \leq \|(u_h^1, \Pi^1 u_h^0)\|_{\Omega_h^1}^2 + \Delta t \sum_{n=0}^1 (\nu \|\nabla u_h^n\|_{\Omega_h^n}^2 + c_{6.6c}K s_2^n(u_h^n, u_h^n)) \\ + (c_{6.6a} + 4\xi + 2\beta) \Delta t \sum_{n=2}^N \|(u_h^{n-1}, \Pi^{n-1} u_h^{n-2})\|_{\Omega_h^{n-1}}^2 + 2\Delta t \beta^{-1} \sum_{n=2}^N \|g^n\|_{\Omega_h^n}^2. \end{aligned}$$

Finally by choosing $\beta = \frac{1}{4}$ and applying the discrete Gronwall's lemma with $\Delta t \xi \leq \frac{1}{16}$ we obtain the result. \square

Let us note that parts of the stability analysis of the unfitted BDF2 method have been treated in a much simplified setting in [11, Section 5.2.1].

6.5. Error estimates.

THEOREM 6.8. *For $u \in \mathcal{L}^\infty(\mathcal{W}_\infty^{k+1})$ with $\partial_t u \in \mathcal{L}^\infty(\mathcal{H}^k)$ and $\partial_t^3 u \in \mathcal{L}^\infty(Q)$ the solution to (2.1) with source term $g \in \mathcal{L}^\infty(\mathcal{W}_\infty^1)$, the numerical solution $\{u_h^n\}$ of (4.12) with $r = 2$ fulfills the error estimate*

$$\begin{aligned} & \|e^N\|_{\Omega_h^N}^2 + \Delta t \sum_{n=2}^N \left(\frac{\nu}{2} \|\nabla e^n\|_{\Omega_h^n}^2 + \gamma s_2^n(e^n, e^n) \right) \\ & \lesssim \exp(c\mathbf{T}) \left((\Delta t^4 + Kh^{2k} + h^{2q}) \mathcal{R}_{6.3}^2 + h^{2k} \mathcal{R}_{6.4}^2 \right) \end{aligned}$$

with $c := c_{6.6a} + 4\xi + 4$ independent of h , Δt and \mathbf{T} .

Proof. By the error splitting (6.3) we have with the interpolation error estimate

$$(6.13) \quad \|e^N\|_{\Omega_h^N}^2 \lesssim \|e_I^N\|_{\Omega_h^N}^2 + \|e_h^N\|_{\Omega_h^N}^2 \lesssim h^{2k} \|u^N\|_{\mathcal{H}^{k+1}(\Omega^N)}^2 + \|e_h^N\|_{\Omega_h^N}^2,$$

hence we only need to bound the last term $\|e_h^N\|_{\Omega_h^N}$. The error equation for e_h^n , (6.7), coincides with (4.12) when replacing u_h^n with e_h^n and $f_h^n(\cdot)$ with $\mathbf{E}_C^n(\cdot) + \mathbf{E}_I^n(\cdot)$. Except for the treatment of the r.h.s. term, we proceed as in Theorem 6.7. We turn our attention to $\mathbf{E}_C^n(\cdot) + \mathbf{E}_I^n(\cdot)$, recall Lemma 6.3 and Lemma 6.4 and sum up:

$$\begin{aligned} & \sum_{n=2}^N \left(\mathbf{E}_C^n(e_h^n) + \mathbf{E}_I^n(e_h^n) \right) \lesssim (\Delta t^2 + K^{\frac{1}{2}} h^k + h^q) \mathcal{R}_{6.3} \sum_{n=2}^N \|e_h^n\|_n + N^{\frac{1}{2}} h^k \mathcal{R}_{6.4} \|e_h^n\|_{L_2} \\ & \lesssim N(\Delta t^4 + Kh^{2k} + h^{2q}) \mathcal{R}_{6.3}^2 + Nh^{2k} \mathcal{R}_{6.4}^2 \\ & \quad + \sum_{n=1}^N \left(\|(\mathbf{e}_h^n, \Pi^n \mathbf{e}_h^{n-1})\|_{\Omega_h^n}^2 + \frac{\nu}{2} \|\nabla \mathbf{e}_h^n\|_{\Omega_h^n}^2 + \gamma s_2^n(\mathbf{e}_h^n, \mathbf{e}_h^n) \right) \end{aligned}$$

Analogously to (6.12) we then arrive at

$$\begin{aligned} & ((1 - 4\Delta t(1 + \xi)) \|(\mathbf{e}_h^N, \Pi^N \mathbf{e}_h^{N-1})\|_{\Omega_h^N}^2 + \Delta t \sum_{n=2}^N \frac{\nu}{2} \|\nabla \mathbf{e}_h^n\|_{\Omega_h^n}^2 + \Delta t \sum_{n=2}^N \gamma s_2^n(\mathbf{e}_h^n, \mathbf{e}_h^n)) \\ & \lesssim \|(\mathbf{e}_h^1, \Pi^1 \mathbf{e}_h^0)\|_{\Omega_h^1}^2 + \Delta t \sum_{n=0}^1 \left(\nu \|\nabla \mathbf{e}_h^n\|_{\Omega_h^n}^2 + \gamma s_2^n(\mathbf{e}_h^n, \mathbf{e}_h^n) \right) + \mathbf{T}(\Delta t^4 + Kh^{2k} + h^{2q}) \mathcal{R}_{6.3}^2 \\ & \quad + \mathbf{T}h^{2k} \mathcal{R}_{6.4}^2 + (c_{6.6a} + 4\xi + 4) \Delta t \sum_{n=2}^N \|(\mathbf{e}_h^{n-1}, \Pi^{n-1} \mathbf{e}_h^{n-2})\|_{\Omega_h^{n-1}}^2. \end{aligned}$$

We apply discrete Gronwall's inequality with $\Delta t(1 + \xi) \leq \frac{1}{8}$ and make use of $\|e_h^N\|_{\Omega_h^N} \leq \|(\mathbf{e}_h^N, \Pi^N \mathbf{e}_h^{N-1})\|_{\Omega_h^N}$, (6.13) and set $c := c_{6.6a} + 4(\xi + 1)$ to obtain the claim. \square

Remark 6.9 (Impact of the anisotropy factor K). The previous error estimate involves the factor $Kh^{2k} \lesssim h^{2k} + \Delta t \cdot h^{2k-1}$. Hence, at first glance it seems that an anisotropy between space and time grid resolution, i.e. when $\Delta t/h \rightarrow \infty$ for $h, \Delta t \rightarrow 0$, can have a negative impact on the convergence rate. For $k > 1$ we can estimate $\Delta t \cdot h^{2k-1} \leq \Delta t^2 \cdot h^k + h^{3k-2} \lesssim \Delta t^4 + h^{2k}$ and can hence conclude that the factor K has no influence on the convergence rates. However, for $k = 1$ we can indeed have that $\Delta t \cdot h$ converges slower than $\Delta t^4 + h^2$ for $\Delta t/h \rightarrow \infty$ for $h, \Delta t \rightarrow 0$.

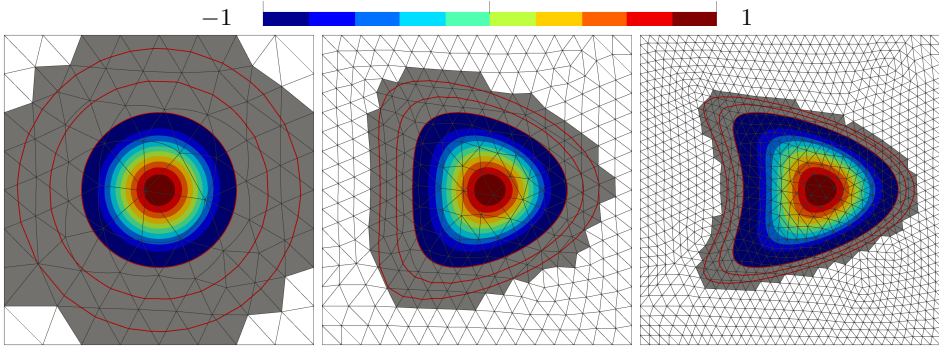


FIG. 7.1. Numerical example from [Subsection 7.1](#) with $k = q = 3$ and $r = 2$ (BDF-2): Mesh, active mesh (grey), neighborhood extension (red line) and discrete solutions on $\Omega(t)$ for $L_x = 0$, $L_t = 3$, $t = 0$ (left), for $L_x = 1$, $L_t = 4$, $t = \mathbf{T}/2$ (center) and $L_x = 2$, $L_t = 5$, $t = \mathbf{T}$ (right).

7. Numerical experiments. In this section we present numerical examples for the method proposed above. The results verify the order of accuracy corresponding to the error analysis, demonstrate the stability with respect to the variation of discretization parameters, and show the robustness to handle evolving domains even in complex configurations. All examples are implemented with the finite element package `NGSolve`[24] and its Add-on `ngsxfem`[22]. For reproducibility of all subsequent numerical results, we provide the generating code and instructions on how to obtain them in the repository <https://gitlab.gwdg.de/lehrenfeld/repro-isop-unf-bdf-fem>.

In slight contrast to the analysis, we make two changes in the discretization. Firstly, use the following bilinear form instead of $b_h^n(u_h, v_h)$: $\int_{\Omega_h^n} \nu \nabla u_h \cdot \nabla v_h \, dx + \int_{\Omega_h^n} (\mathbf{w}^e \cdot \nabla u_h) v_h \, dx + \int_{\Omega_h^n} (\operatorname{div} \mathbf{w}^e) u_h v_h \, dx$. Secondly, we do not include the additional element layers for the extension, i.e., we skip the “+” layers defined in [Subsection 3.2](#). However, in all subsequent numerical examples we ensured that the desired inclusion properties hold. In the examples we consider an additional source term in order to simplify the construction of manufactured solutions. We hence add a linear form $f_h^n(v_h) := \int_{\Omega_h^n} g v_h \, dx$ to the right hand side of the discrete variational formulation.

Related to the previous error analysis, we investigate the numerical errors in terms of the following discrete space-time norms

$$(7.1) \quad \|\mathbf{e}\|_{\mathcal{L}^2(\mathcal{H}^1)}^2 := \sum_{n=1}^N \Delta t \|\nabla \mathbf{e}\|_{\mathcal{L}^2(\Omega_h^n)}^2, \quad \|\mathbf{e}\|_{\mathcal{L}^\infty(\mathcal{L}^2)} := \max_{n=1, \dots, N} \|\mathbf{e}\|_{\mathcal{L}^2(\Omega_h^n)}, \quad \mathbf{e} = u - u_h,$$

where we recall that u is identified with its extension u^e to the suitable neighborhood. For each example we start with an initial (quasi-uniform) spatial and (uniform) temporal mesh with mesh size h_0 and Δt_0 , respectively, and then apply successive regular refinements in space and time. We denote the corresponding refinement levels in space by L_x , and those in time by L_t , s.t. $h = h_0 \cdot 2^{-L_x}$, $\Delta t = \Delta t_0 \cdot 2^{-L_t}$.

7.1. Kite geometry. In this first example we consider a disk deforming towards a kite shape, cf. [Figure 7.1](#). The background domain is fixed to $\tilde{\Omega} = (-1, 1)^2$ and the final time in the simulation to $\mathbf{T} = 1$. The evolution of the geometry is represented by the following level set function ϕ :

$$\phi(\mathbf{x}, t) = \|\mathbf{x} - \rho(\mathbf{x}, t)\|_2 - \frac{1}{2} \quad \text{with } \rho(\mathbf{x}, t) = \mathbf{w}(\mathbf{x}) \cdot t, \quad \mathbf{w} = (1/6 - 5/3y^2, 0)^T.$$

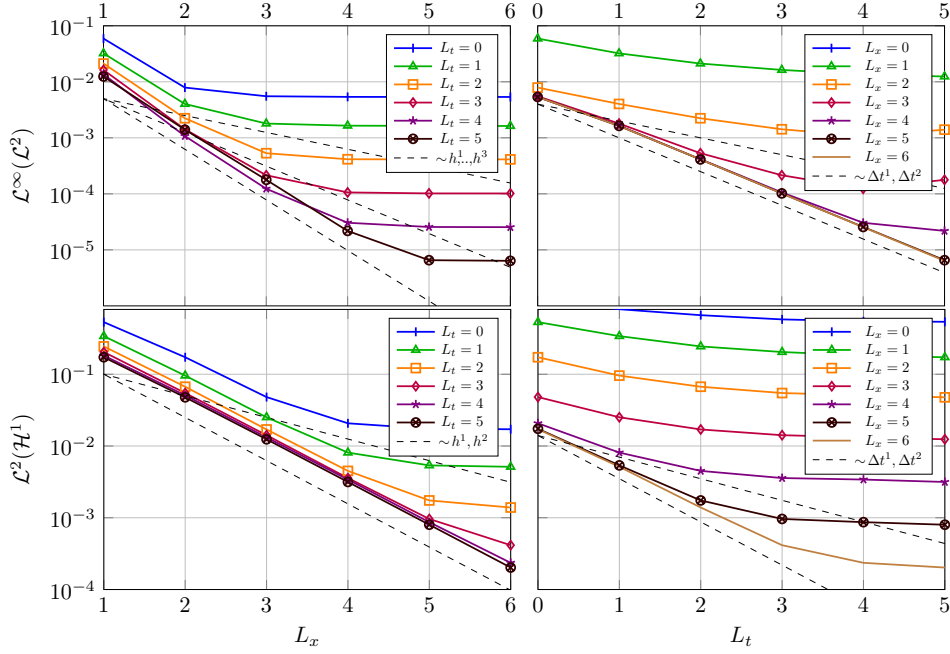


FIG. 7.2. $\mathcal{L}^\infty(\mathcal{L}^2)$ - and $\mathcal{L}^2(\mathcal{H}^1)$ -errors of BDF-2 discretization for $k = q = 2$ and $c_\gamma = 0.1$ for several levels of mesh and time refinements in the example from Subsection 7.1.

Note that ϕ is not a signed distance function for $t > 0$. The r.h.s. function g is set so that $u(\mathbf{x}, t) = \cos \frac{\pi}{R} \|\mathbf{x} - \rho(\mathbf{x}, t)\|_2$ (which has $-\nabla u \cdot \mathbf{n} = 0$, on $\Gamma(t)$, $t \in [0, \mathbf{T}]$) solves the PDE. The initial spatial and temporal resolutions are $h_0 = 0.25$ and $\Delta t_0 = \mathbf{T}$.

In Figure 7.2 the convergence of the error norms $\mathcal{L}^\infty(\mathcal{L}^2)$ and $\mathcal{L}^2(\mathcal{H}^1)$ are displayed for $r = k = q = 2$ and we observe that the convergence rate in time is Δt^2 in both norms whereas the convergence rate in space is h^2 in $\mathcal{L}^2(\mathcal{H}^1)$ and h^3 in $\mathcal{L}^\infty(\mathcal{L}^2)$. These results are in agreement with the previous analysis except for the h^3 convergence in $\mathcal{L}^\infty(\mathcal{L}^2)$ which is even one order better than predicted.

7.2. Two-phase mass transport. We finally consider a more complex example that is beyond the scope of the previous analysis and third order methods in space and time. In this example we consider a two-phase interface problem as in [14]. A circular interface that separates two materials is moving within the background domain $\Omega = (0, 2)^2$ for $t \in [0, \mathbf{T}]$, $\mathbf{T} = \frac{1}{2}$. The two domains are described by the level set function $\phi(\mathbf{x}, t) = \|\mathbf{x} - \rho(t)\|_2 - \frac{1}{3}$ with $\rho(t) = (\frac{1}{2} + \frac{1}{4\pi} \sin(2\pi t), 1)$ which describes a circle moving with time-dependent velocity in the horizontal direction. We define $\Omega_1(t) = \{\phi(\mathbf{x}, t) < 0\}$, $\Omega_2(t) = \{\phi(\mathbf{x}, t) > 0\}$. On both subdomains the convection-diffusion equation $\partial_t u + \mathbf{w} \cdot \nabla u - \nu_i \Delta u = g$, $\mathbf{w} = \partial_t \rho(t)$ is solved. We prescribe Dirichlet data on $\partial\Omega$ and writing $[[w]] = w_1 - w_2$ for the jump, and impose the interface conditions $[-\nu \nabla u \cdot \mathbf{n}] = 0$, $[[\beta u]] = 0$ on $\Gamma(t) = \overline{\Omega}_1(t) \cap \overline{\Omega}_2(t)$ for ν_i , $i = 1, 2$ the diffusion constants and β_i , $i = 1, 2$ the Henry weights for the Henry interface condition. We choose $(\nu_1, \nu_2) = (10, 20)$ and $(\beta_1, \beta_2) = (2, 1)$. The corresponding boundary data and r.h.s. data f is prescribed such that $u(\mathbf{x}, t) = \sin(\pi t) u_i(\|\mathbf{x} - \rho(t)\|)$ with $u_1(r) = a + br^2$ and $u_2(r) = \cos(\pi r)$, $a \approx 1.1569$, $b \approx -8.1621$, is the unique solution.

For the discretization we use an unfitted discretization similar to (4.12), but for

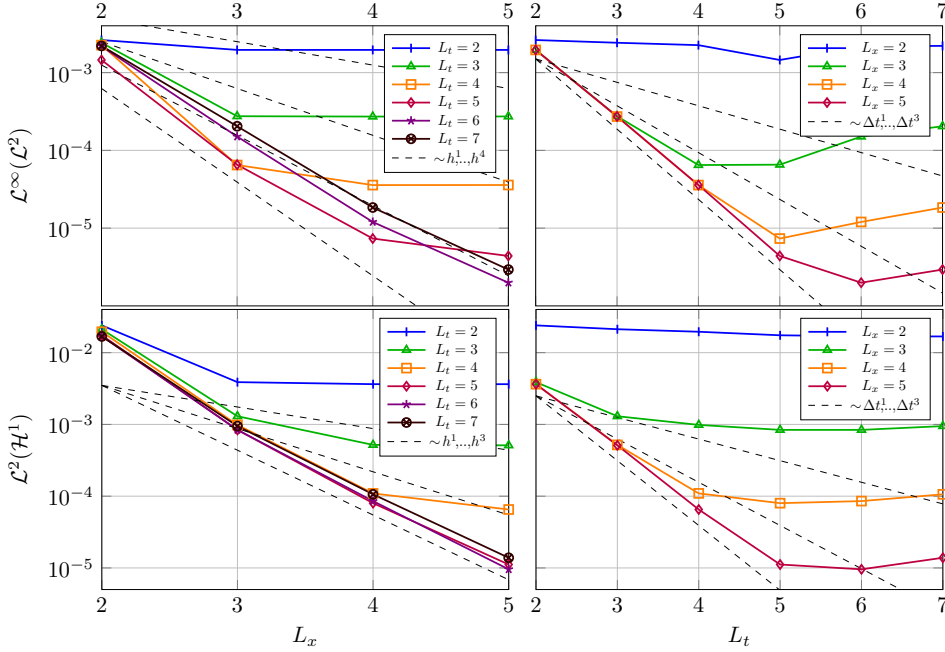


FIG. 7.3. $\mathcal{L}^\infty(\mathcal{L}^2)$ - and $\mathcal{L}^2(\mathcal{H}^1)$ -errors of BDF-3 discretization for $k = q = 3$ and $c_\gamma = 10$ for several levels of mesh and time refinements in the example from Subsection 7.2.

both subdomains with a Nitsche formulation for the coupling through the interface conditions. The discretization takes the form:

Find $u_h^n = (u_{1,h}^n, u_{2,h}^n) \in \mathcal{V}_{r,1}^n \times \mathcal{V}_{r,2}^n$, $n = r, \dots, N$ for given $u_{i,h}^0 \in \mathcal{V}_{r,i}^0, \dots, u_{i,h}^{r-1} \in \mathcal{V}_{r,i}^{r-1}$, $i = 1, 2$, s.t. for all $v_h = (v_{1,h}, v_{2,h}) \in \mathcal{V}_{r,1}^n \times \mathcal{V}_{r,2}^n$ there holds

$$\begin{aligned} & \sum_{i=1,2} \beta_i \left\{ \int_{\Omega_{i,h}^n} \partial_{\Delta t}^r (u_{i,h}^n, \dots, \Pi_{n-r}^n u_{i,h}^{n-r}) v_h \, dx + b_{i,h}^n(u_h^n, v_h) + \gamma s_{i,r}^n(u_h^n, v_h) \right\} \\ & + \int_{\Gamma} -\{\nu \nabla u_h \cdot n_\Gamma\} \llbracket \beta v_h \rrbracket - \{\nu \nabla v_h \cdot n_\Gamma\} \llbracket \beta u_h \rrbracket + \frac{\{\nu\} \lambda_N}{h} \llbracket \beta u_h \rrbracket \llbracket \beta v_h \rrbracket \, ds = \sum_{i=1,2} \beta_i \int_{\Omega_{i,h}^n} g_i v_{i,h} \, dx, \end{aligned}$$

where $\Omega_{i,h}^n$ is the discrete geometry approximation to $\Omega_i(t^n)$ as previously, g_i is a proper extension of $g|_{\Omega_i}$ to $\Omega_{i,h}^n$, and $b_{i,h}^n(\cdot, \cdot)$, $s_{i,r}^n(\cdot, \cdot)$ are the bilinear forms analogously to before, but now acting on $\Omega_{i,h}^n$ and on a corresponding set of facets $\mathcal{F}_{i,r}^n$, respectively. In the Nitsche terms, we used $\{\{w\}\} := \frac{w_1 + w_2}{2}$ and for λ_N we choose 40. The spatial and temporal resolution are $h_0 = 0.5$ and $\Delta t_0 = \mathbf{T}$ initially.

In Figure 7.3 the convergence of the error norms $\mathcal{L}^\infty(\mathcal{L}^2)$ and $\mathcal{L}^2(\mathcal{H}^1)$ (which are composed as the summation of the corresponding norms on the subdomains $i = 1, 2$) are displayed for $r = k = q = 3$ and we observe that the convergence rate in time is Δt^3 in both norms whereas the convergence rate in space is h^3 . The convergence rate in space in the $\mathcal{L}^\infty(\mathcal{L}^2)$ norm is even higher. Again, these results are in agreement with the expectations from the case of only one moving domain.

8. Conclusion. In this paper we have extended the numerical method from [17] for solving PDEs on evolving domains towards *provably* higher order of accuracy in space and time. The method shows several advantages over its competitors aforementioned in Section 1. In comparison to the space-time approach, the proposed method

based on the standard isoparametric unfitted FEM involves only spatial integrals and finite element spaces, which leads to an implementational and computational complexity that is comparable to stationary unfitted problems. While compared to the characteristic Galerkin scheme, the method trades the extra cost and complexity of the Lagrangian tracking of the geometry (to high-order accuracy) with a comparably simple ghost-penalty-based discrete extension. The extension compared to [17] consists of the combination of the Eulerian time stepping with the isoparametric unfitted FEM in space and its analysis on the one hand and the extension of the analysis from an implicit Euler to a BDF scheme on the other hand.

Acknowledgments. The authors gratefully acknowledge funding by the DFG (German Research Foundation) within the project ‘‘LE 3726/1-1’’.

Appendix A. Selected proofs.

Proof of Lemma 5.4. Let us consider a facet $F^n \in \mathcal{F}_1^n$ with the corresponding uncurved facet $\hat{F} = \Theta^{-n}(F^n)$ and hence $F^m = \Theta^m(\hat{F}) \in \mathcal{F}_2^m$. Their adjacent elements of the patches are denoted as $\omega(F^n) = T_1^n \cup T_2^n$, $\hat{\omega}(\hat{F}) = \hat{T}_1 \cup \hat{T}_2$, and $\omega(F^m) = T_1^m \cup T_2^m$, respectively. Note that $\Theta_{T_1}^m$, $\Theta_{T_1}^n$, $\Theta_{T_2}^m$ and $\Theta_{T_2}^n$ are involved here. Let $u_h = \Pi^n v_h \in \mathcal{V}_h^n$ be the discrete function after projection and recall the notation from Subsection 4.1, i.e. $u_i = \hat{u}_i \circ \Theta_{T_i}^{-n*}$, $i = 1, 2$ with $\hat{u}_i := \mathcal{E}^{\mathcal{P}}(u_h|_{T_i^n} \circ \Theta_{T_i}^n)$ and $v_i = \hat{v}_i \circ \Theta_{T_i}^{-m*}$, $i = 1, 2$ with $\hat{v}_i := \mathcal{E}^{\mathcal{P}}(v_h|_{T_i^m} \circ \Theta_{T_i}^m)$. We further introduce the notation for the properly extended neighbor functions: $\hat{u}_j^* := \hat{u}_j \circ \Upsilon^n(\hat{x})$ and $\hat{v}_j^* := \hat{v}_j \circ \Upsilon^m(\hat{x})$ with $\Upsilon^n = \Theta_{T_j}^{-n*} \circ \Theta_{T_i}^n$ and $\Upsilon^m = \Theta_{T_j}^{-m*} \circ \Theta_{T_i}^m$. Taking the definition of the ghost penalty from (4.3) and exploiting the smallness of the deformations, we find after transformation to \hat{T}_i, \hat{T}_j

$$h^2 s_F^n(u_h, u_h) \leq 2 \sum_{i,j=1,2} \int_{\hat{T}_i} (\hat{u}_i - \hat{u}_j^*)^2 d\hat{x} \text{ and } \sum_{i,j=1,2} \int_{\hat{T}_i} (\hat{v}_i - \hat{v}_j^*)^2 d\hat{x} \leq 2h^2 s_F^m(v_h, v_h).$$

Let $a := \hat{u}_i - \hat{u}_j^*$ and $b := \hat{v}_i - \hat{v}_j^*$. Then with $A := \hat{u}_i - \hat{v}_i$ and $B := \hat{u}_j^* - \hat{v}_j^*$ we have $a - b = A - B$ so that there holds

$$\begin{aligned} a^2 - b^2 &= \underbrace{(a - b)}_{(A-B)}(a + b) \leq (A - B)^2 + \frac{1}{4}(a + b)^2 \leq 2(A^2 + B^2) + \frac{1}{2}(a^2 + b^2) \\ &\implies \frac{1}{2}a^2 - \frac{3}{2}b^2 \leq 2(A^2 + B^2) \implies a^2 \leq 3b^2 + 4(A^2 + B^2). \end{aligned}$$

Hence, we obtain

$$s_F^n(u_h, u_h) \lesssim s_F^m(v_h, v_h) + h^{-2} \sum_{\substack{i,j=1,2 \\ i \neq j}} \left(\underbrace{\|\hat{u}_i - \hat{v}_i\|_{\hat{T}_i}^2}_{=A} + \underbrace{\|\hat{u}_i^* - \hat{v}_i^*\|_{\hat{T}_i}^2}_{=B} \right)$$

As a polynomial in $\mathcal{P}^k(\mathbb{R}^d)$ we can retreat $A(\hat{x})$ to $\hat{T}_{i,-\varepsilon}$ and find

$$\begin{aligned} \|A\|_{\hat{T}_i} &\simeq \|A\|_{\hat{T}_{i,-\varepsilon}} \lesssim \|v_h \circ \Theta_{T_i}^n - \overbrace{u_h \circ \Theta_{T_i}^n}^{\hat{u}_i}\|_{\hat{T}_{i,-\varepsilon}} + \|v_h \circ \Theta_{T_i}^n - \overbrace{v_h \circ \Theta_{T_i}^n}^{\hat{v}_i}\|_{\hat{T}_{i,-\varepsilon}} \\ &\lesssim \|(\text{id} - \Pi^n)v_h\|_{T_i^n} + \|v_h \circ (\Theta_{T_i}^n - \Theta_{T_i}^m)\|_{\hat{T}_{i,-\varepsilon}} \lesssim h^2 \|\nabla v_h\|_{\omega(T_i^m)} \end{aligned}$$

where in the last step we made use of Lemma 5.3 and the closeness of Θ_T^n and Θ_T^m . For $B(\hat{x})$ we first note that $\|\Upsilon^n - \Upsilon^m\|_{\mathcal{L}^\infty(\hat{T}_i)} \lesssim h^2$ and recall that $\hat{u}_j - \hat{v}_j \in \mathcal{P}^k(\mathbb{R}^d)$

s.t. with standard scaling arguments we have $\|\hat{u}_j - \hat{v}_j\|_{\Upsilon^n(\hat{T}_i)} \lesssim \|\hat{u}_j - \hat{v}_j\|_{\hat{T}_{j,-\varepsilon}}$ and

$$\begin{aligned} \|B\|_{\hat{T}_i} &\lesssim \|(\hat{u}_j - \hat{v}_j) \circ \Upsilon^n\|_{\hat{T}_i} + \|\hat{v}_j \circ \Upsilon^n - \hat{v}_j \circ \Upsilon^m\|_{\hat{T}_j} \lesssim \|\hat{u}_j - \hat{v}_j\|_{\Upsilon^n(\hat{T}_i)} + h^2 \|\nabla v_h\|_{T_j^m} \\ &\lesssim \|u_h \circ \Theta_{T_j}^n - v_h \circ \Theta_{T_j}^m\|_{\hat{T}_{j,-\varepsilon}} + h^2 \|\nabla v_h\|_{T_j^m} \\ &\lesssim \|(u_h - v_h) \circ \Theta_{T_j}^n\|_{\hat{T}_{j,-\varepsilon}} + \|v_h \circ \Theta_{T_j}^n - v_h \circ \Theta_{T_j}^m\|_{\hat{T}_{j,-\varepsilon}} + h^2 \|\nabla v_h\|_{T_j^m} \\ &\lesssim \|\Pi^n u_h - v_h\|_{T_j^n} + h^2 \|\nabla v_h\|_{T_j^m} \lesssim h^2 \|\nabla v_h\|_{\omega(T_j^m)}. \end{aligned}$$

Putting all together yields the proof. \square

Proof of Lemma 6.3. Recall (6.6), i.e. $\mathbf{E}_C^n(v_h) = \sum_{i=1}^4 \mathbf{E}_C^{n,i}(v_h)$. We start with $\mathbf{E}_C^{n,1}(v_h)$ by triangle inequality

$$|\mathbf{E}_C^{n,1}(v_h)| \leq \underbrace{\left| \int_{\Omega_h^n} \left(\partial_{\Delta t}^2(u^n, u^{n-1}, u^{n-2}) - \partial_t u^n \right) v_h dx \right|}_{\mathbf{E}_C^{n,a}} + \underbrace{\left| \int_{\Omega_h^n} \partial_t u^n v_h dx - \int_{\Omega^n} \partial_t u^n v_h^\ell dx \right|}_{\mathbf{E}_C^{n,b}}.$$

The first term is similar to the one in [17, Lemma 5.11] but differs due to the high-order time difference stencil. By elementary calculations based on partial integration on $[t_{n-2}, t_{n-1}]$ and $[t_{n-1}, t_n]$ one obtains

$$\mathbf{E}_C^{n,a} = \int_{\Omega_h^n} \int_{t_{n-2}}^{t_n} z(t) \partial_t^3 u \, dt \, v_h \, dx$$

for $z \in C^1([t_{n-2}, t_n])$ satisfying $z(t)|_{[t_{n-2}, t_{n-1}]} = -\frac{1}{4\Delta t}(t - t_{n-2})^2$ and $z(t)|_{(t_{n-1}, t_n]} = \frac{1}{12\Delta t}((3t - t_{n-1} - \Delta t)^2 - 4\Delta t^2)$ and hence $\|z\|_{\mathcal{L}^\infty([t_{n-2}, t_n])} \leq \frac{1}{3}\Delta t$. We have with $\|\partial_t^3 u\|_{\mathcal{L}^\infty(\Omega_h^n \times [t_{n-2}, t_n])} \leq \|\partial_t^3 u\|_{\mathcal{L}^\infty(Q_\varepsilon)} \leq \|\partial_t^3 u\|_{\mathcal{L}^\infty(Q)}$ the bound

$$\mathbf{E}_C^{n,a} \lesssim \Delta t^2 \|\partial_t^3 u\|_{\mathcal{L}^\infty(Q)} \|v_h\|_{\Omega_h^n}.$$

The second term $\mathbf{E}_C^{n,b}$ involves the high-order geometrical approximation error, i.e. the error from $\Omega_h^n := \Theta(\Omega_{\hat{\phi}_h}^n)$. By notating $\Phi := \Psi \circ \Theta^{-1} : \Omega_h^n \rightarrow \Omega^n$, i.e., a mapping from the discrete domain to the exact domain, and applying an integral transformation we have

$$|\mathbf{E}_C^{n,b}| = \left| \int_{\Omega_h^n} (\partial_t u^n - (\partial_t u^n \circ \Phi) \det(D\Phi)) v_h dx \right|$$

Splitting the integrand (expect for the factor v_h) into the sum of $\partial_t u^n - (\partial_t u^n \circ \Phi)$ and $(\partial_t u^n \circ \Phi)(1 - \det(D\Phi))$ yields

$$\begin{aligned} |\mathbf{E}_C^{n,b}| &\leq \left| \int_{\Omega_h^n} |\text{id} - \Phi| \|\nabla \partial_t u\|_{\mathcal{L}^\infty(\Omega_h^n)} v_h dx \right| + \left| \int_{\Omega_h^n} |1 - \det(D\Phi)| \|\partial_t u\|_{\mathcal{L}^\infty(\Omega_h^n)} v_h dx \right| \\ &\lesssim h^{q+\frac{1}{4}} \|u\|_{\mathcal{W}_\infty^2(Q)} \|v_h\|_{\mathcal{L}^1(\Omega_h^n)} + h^q \|u\|_{\mathcal{W}_\infty^1(Q)} \|v_h\|_{\mathcal{L}^1(\Omega_h^n)} \lesssim h^q \|u\|_{\mathcal{W}_\infty^2(Q)} \|v_h\|_{\Omega_h^n}, \end{aligned}$$

where we made use of

$$|\partial_t u^n(x) - (\partial_t u^n \circ \Phi)(x)| \leq \|\nabla \partial_t u\|_{\mathcal{L}^\infty(\Omega_h^n)} |x - \Phi(x)|$$

and Lemma 3.3 to bound the geometrical errors.

The bound for the second part follows similar lines in [17, Lemma 5.11] and yields

$$|\mathbf{E}_C^{n,2}(v_h)| = |b_h^n(u^n, v_h) - b^n(u^n, v_h^\ell)| \lesssim h^q \|u\|_{\mathcal{W}_\infty^2(Q)} \|v_h\|_{\mathcal{H}^1(\Omega_h^n)}.$$

The third part is obtained with a Cauchy-Schwarz inequality and the estimate from [17, Lemma 5.8], which is still valid on deformed meshes.

$$\begin{aligned} \mathbf{E}_C^{n,3}(v_h) &= \gamma s_2^n(u^n, v_h) \leq \gamma s_2^n(u^n, u^n)^{\frac{1}{2}} s_2^n(v_h, v_h)^{\frac{1}{2}} \\ &\lesssim \gamma h^k \|u^n\|_{\mathcal{H}^{k+1}(\mathcal{O}_{h,2}^n)} s_2^n(v_h, v_h)^{\frac{1}{2}} \lesssim K^{\frac{1}{2}} h^k \|u^n\|_{\mathcal{H}^{k+1}(\Omega^n)} (\gamma s_2^n(v_h, v_h))^{\frac{1}{2}}, \end{aligned}$$

where for the last inequality we make use of $\mathcal{O}_{h,2}^n \subset \Omega_\epsilon^n$ and continuity of the extension.

Finally, the fourth part is estimated analogously to $|\mathbf{E}_C^{n,b}|$ as follows

$$\begin{aligned} |\mathbf{E}_C^{n,4}(v_h)| &= \left| \int_{\Omega_h^n} ((g \circ \Phi) \det(D\Phi) - g) v_h \, dx \right| \leq \|v_h\|_{\mathcal{L}^1(\Omega_h^n)} \cdot \\ &\quad \cdot (\|1 - \det(D\Phi)\|_{\mathcal{L}^\infty(\Omega_{h,\epsilon}^n)} \|g\|_{\mathcal{L}^\infty(\Omega_{h,\epsilon}^n)} + \|\text{id} - \Phi\|_{\mathcal{L}^\infty(\Omega_{h,\epsilon}^n)} \|\nabla g\|_{\mathcal{L}^\infty(\Omega_{h,\epsilon}^n)}) \\ &\lesssim (h^q \|g\|_{\mathcal{L}^\infty(\Omega_h^n)} + h^{q+1} \|g\|_{\mathcal{W}_\infty^1(\Omega_h^n)}) \cdot \|v_h\|_{\Omega_h^n} \lesssim \sup_{t \in [0, \mathbf{T}]} h^q \|g\|_{\mathcal{W}_\infty^1(\Omega(t))} \|v_h\|_{\Omega_h^n}. \quad \square \end{aligned}$$

REFERENCES

- [1] E. BURMAN, *Ghost penalty*, C. R. Math. Acad. Sci. Paris, 348 (2010), pp. 1217–1220.
- [2] E. BURMAN, S. CLAUS, P. HANSBO, M. G. LARSON, AND A. MASSING, *Cutfem: Discretizing geometry and partial differential equations*, International Journal for Numerical Methods in Engineering, 104 (2015), pp. 472–501.
- [3] E. BURMAN, S. FREI, AND A. MASSING, *Eulerian time-stepping schemes for the non-stationary stokes equations on time-dependent domains*, arXiv preprint arXiv:1910.03054, (2020).
- [4] Q. Z. CHUWEN MA AND W. ZHENG, *A high-order fictitious-domain method for the advection-diffusion equation on time-varying domain*, arXiv preprint arXiv:2104.01870, (2020).
- [5] A. ERN AND J.-L. GUERMOND, *Theory and practice of finite elements*, Springer, New York, 2004.
- [6] T. FRACHON AND S. ZAHEDI, *A cut finite element method for incompressible two-phase navier-stokes flows*, Journal of Computational Physics, 384 (2019), pp. 77–98.
- [7] J. GRANDE, C. LEHRENFELD, AND A. REUSKEN, *Analysis of a high-order trace finite element method for PDEs on level set surfaces*, SIAM Journal on Numerical Analysis, 56 (2018), pp. 228–255.
- [8] P. HANSBO, M. G. LARSON, AND S. ZAHEDI, *Characteristic cut finite element methods for convection–diffusion problems on time dependent surfaces*, Computer Methods in Applied Mechanics and Engineering, 293 (2015), pp. 431–461.
- [9] ———, *A cut finite element method for coupled bulk–surface problems on time-dependent domains*, Computer Methods in Applied Mechanics and Engineering, 307 (2016), pp. 96–116.
- [10] F. HEIMANN, *On Discontinuous- and Continuous-In-Time Unfitted Space-Time Methods for PDEs on Moving Domains*, master’s thesis, NAM, University of Göttingen, 2020.
- [11] X. JIN, *Higher order stabilized time stepping in unfitted finite element method on moving domains*, master’s thesis, NAM, University of Göttingen, 2019.
- [12] P. L. LEDERER, C.-M. PFEILER, C. WINTERSTEIGER, AND C. LEHRENFELD, *Higher order unfitted FEM for Stokes interface problems*, PAMM, 16 (2016), pp. 7–10.
- [13] C. LEHRENFELD, *The Nitsche XFEM-DG space-time method and its implementation in three space dimensions*, SIAM J. Sci. Comp., 37 (2015), pp. A245–A270.
- [14] C. LEHRENFELD, *On a Space-Time Extended Finite Element Method for the Solution of a Class of Two-Phase Mass Transport Problems*, PhD thesis, RWTH Aachen, February 2015.
- [15] C. LEHRENFELD, *High order unfitted finite element methods on level set domains using isoparametric mappings*, Comp. Meth. Appl. Mech. Eng., 300 (2016), pp. 716–733.
- [16] ———, *A higher order isoparametric fictitious domain method for level set domains*, in Geometrically Unfitted Finite Element Methods and Applications, S. P. A. Bordas, E. Burman,

- M. G. Larson, and M. A. Olshanskii, eds., Springer International Publishing, 2017, pp. 65–92.
- [17] C. LEHRENFELD AND M. A. OLSHANSKII, *An Eulerian finite element method for PDEs in time-dependent domains*, ESAIM: M2AN, 53 (2019), pp. 585–614.
 - [18] C. LEHRENFELD AND A. REUSKEN, *Analysis of a Nitsche XFEM-DG discretization for a class of two-phase mass transport problems*, SIAM J. Numer. Anal., 51 (2013), pp. 958–983.
 - [19] ———, *l^2 -estimates for a high order unfitted finite element method for elliptic interface problems*, arXiv preprint arXiv:1604.04529, (2016).
 - [20] ———, *Analysis of a high order unfitted finite element method for an elliptic interface problem*, IMA J. Numer. Anal., 38 (2018), pp. 1351–1387.
 - [21] J. LIU, *Simple and efficient ale methods with provable temporal accuracy up to fifth order for the stokes equations on time varying domains*, SIAM Journal on Numerical Analysis, 51 (2013), pp. 743–772.
 - [22] *ngsxfem : Add-On to NGSolve for unfitted finite element methods*. <http://github.com/ngsxfem>.
 - [23] J. PREUSS, *Higher order unfitted isoparametric space-time FEM on moving domains*, master's thesis, NAM, University of Göttingen, 2018.
 - [24] J. SCHÖBERL, *C++11 Implementation of Finite Elements in NGSolve*, Institute for Analysis and Scientific Computing, Vienna University of Technology, (2014).
 - [25] B. SCHOTT, *Stabilized Cut Finite Element Methods for Complex Interface Coupled Flow Problems*, phd thesis, TU Munich, 2017.
 - [26] H. VON WAHL, T. RICHTER, AND C. LEHRENFELD, *An unfitted eulerian finite element method for the time-dependent stokes problem on moving domains*, arXiv preprint arXiv:2002.02352, (2020).
 - [27] S. ZAHEDI, *A space-time cut finite element method with quadrature in time*, in Geometrically Unfitted Finite Element Methods and Applications, Springer, 2017, pp. 281–306.